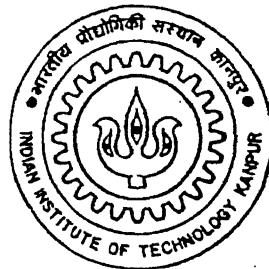# FEM Simulation of Ultrasonic NDT for Defect Characterization in Tubes.

A Thesis Submitted

in Partial Fulfillment of the Requirements

for the Degree of

Master of Technology

by

Santosh N. Kulkarni

to the

DEPARTMENT OF MECHANICAL ENGINEERING

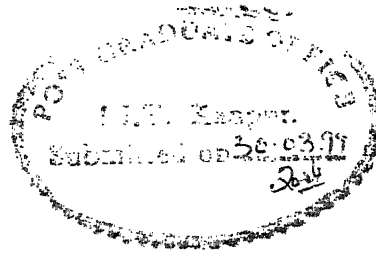## INDIAN INSTITUTE OF TECHNOLOGY, KANPUR

March, 1999

Dedicated

to

My Teachers

CERTIFICATE

*It is certified that the work contained in the thesis entitled **FEM Simulation of Ultrasonic NDT for Defect Characterization in Tubes** by **Santosh N. Kulkarni** has been carried out under my supervision and this work has not been submitted elsewhere for a degree.*

Dr. N.N. Kishore

Professor,

Dept. of Mechanical Engg,

Indian Institute of Technology,

Kanpur 208016.

Acknowledgements

I would like to express my deep sense of gratitude to Dr. N.N. Kishore for his invaluable guidance throughout my M.Tech programme. It is because of his constant encouragement and motivation, I could accomplish some fruitful results in my thesis work. His vast experience and immense knowledge in the field of FEM and Wave Propagation were always found to be path finder at each difficult stage. I am always greatful to him for sparing his precious time and providing valuable suggestions at each point.

I would like to pay my sincere regards to Mr. S.K. Rathore, Mr. S.K. Singhal, Mr. Atul Agrawal and Mr. S. Ravi for giving constant motivation and encouragement during the thesis work. Special thank goes to Mr. S.K. Rathore for providing useful suggestions and new ideas during the thesis work.

I am thankful to all of my classmates and friends for giving me a good company and making my stay at IIT Kanpur a pleasant and memorable one.

<div align="right">

Santosh N. Kulkarni.

</div>

Abstract

Ultrasonic Testings are popular techniques for the Non-destructive testing of the load bearing components. For engineering components such as long pipes, it is beneficial to develop an inspection method which can cover the entire length without moving the transducer. Recently developed guided waves are gaining a lot of importance because of their excellent penetration capability and sensitivity to defects. These can be simulated by the Finite Element modeling of the wave propagation in elastic solids.

In the present work, an inspection methodology has been developed for the detection and characterization of cracks in tubes having circumferential orientation. The phenomenon of guided waves and their mode conversion is exploited for the defect detection. The tube is excited in the longitudinal mode by a short duration axisymmetric loading pulse. Because of the presence of non-axisymmetric cracks, various flexural modes will also be generated. The displacement field is monitored and processed to get the converted modes which reveal the information about the crack geometry.

The amplitude of the longitudinal mode is found to be varying linearly with respect to the size of the crack. And the magnitudes of the flexural modes are found to be very small for axisymmetric defects. Using the present method, results of number of cases are obtained. The present method is applied to analyze circumferential cracks and the work can be extended for the defects having angular orientations.

Contents

List of Figures

List of Symbols

x, y, z Global coordinates

ξ, η, ζ Local coordinates

u_i Displacements components in local system

$\{\epsilon\}$ Strain matrix

$\{\sigma\}$ Stress matrix

μ, λ Lame's constants

ρ Density

ϕ Scalar potential field

$\underline{\psi}$ Vector potential field

k Wavenumber

ω Frequency in rad/sec

h Layer thickness

C_l, C_t Longitudinal and shear wave speed

Π Total potential energy

N_i Shape functions

t Shell thickness

$\{u\}^{(e)}$	Elemental displacement matrix
$\{\dot{u}\}^{(e)}$	Elemental velocity matrix
$\{\ddot{u}\}^{(e)}$	Elemental acceleration matrix
P_B	Body force
P_S	Surface traction
Γ_σ	Surface traction boundary
E	Elastic modulus
ν	Poisson's ratio
k_f	Factor to improve the strain displacement approximation
[D]	Material property matrix
[K]	Stiffness matrix
[M]	Mass matrix

Chapter 1

Introduction

1.1 Introduction

Non destructive testing has attracted great deal of attention because of its quality, simplicity and reliability. Several NDE methods such as bulk wave ultrasonics, radiography, eddy currents, visual optics are used in practice. Recently developed, ultrasonic guided waves are becoming popular for the simulation of the ND technique for the defect detection and characterization. This is because of their excellent penetration capability and sensitivity to defects. These are also capable of inspecting entire length of the structure without moving the ultrasonic transducer.

Tube inspection technology plays a vital role in various engineering fields such as nuclear power plant, petroleum and natural gas plants where the safety is of atmost importance. Some of the commonly faced problems in tubes are radial wear, sizing, wall thinning and leakages. Recently, with ongoing need of the safety standards in nuclear power plants, Ministry of International Trade and Industry, Japan has instituted a project "Development and Verification of Inspection Techniques for Steam Generator Tubes." It is supposed to develop a full length inspection technique for the tubes.

For thin structures, with the use of bulk waves, it is indeed difficult to study the exact nature of reflections and transmissions at the boundary interference. And specially for the axisymmetric components, such as bars, tubes and cylinders, it is almost impossible to trace

the reflections from the boundaries. In such cases, it is possible to define the standing waves across the thickness of the structure and propagating along a certain direction. These are known as guided waves and is the obvious choice for the NDT of thin walled structures. The investigation of the guided waves lead to introduction of several new concepts of modes of propagation, frequency spectrum, dispersion phenomenon and group velocity.

1.2 Literature Survey

Recent developments in the high speed computing machines, their data storage facility and the simulation capabilities made it possible the simulation of the ND testing. Also in recent years, great efforts have been made in presenting suitable mathematical models which can represent the exact nature of the non destructive techniques.

The first general solution of the harmonic wave propagation in infinitely long elastic cylinders was obtained by Gazis et al [1] by using the elasticity theory. Ultrasonic guided wave propagation in hollow cylinders was studied by Fitch [2]. Transient vibratory response of a fluid loaded shell with axisymmetric excitation was studied by Stepanishen et al [3]. Brunetal et al [4] applied a direct integration approach for the study of circumferential SH waves in hollow cylinders. Longitudinal and transverse mode phenomenon for the inspection of welds was studied by Neumann [5]. The effects of incident angle and wavelength in the ultrasonic testing was elaborated by Kalkhof et al [6]. To simulate the 3-D nature of the defects in tubes, Monbhurrun et al [7] proposed an integral formulation of the wavefield by Green's dyadic function.

Due to the geometry of the tube, modes can be broadly classified into two types, axisymmetric and non-axisymmetric modes. Great progress is being made on both the types of modes for the inspection of tubes. Axisymmetric modes are used for analytical simplicity and easier signal processing of the waveforms. But for the complex nature of the crack geometry and orientation of the crack, the study of non-axisymmetric modes cannot be avoided.

Considerable work has been done on using the Lamb waves in tubing inspection. There are some difficulties in using Lamb waves due to the presence of a number of modes and the dispersion effect. Lowe [9] determined the dispersion curves and mode shapes for flat or cylindrical structures with arbitrary number of layers. The modes are labeled as: longitudinal ("L"), flexural ("F") and torsional ("T") after the convention of Silk et al [10]. They used piezoelectric ultrasonic probes to access the inside of the tube. Rose et al [11] employed the mode control concept and reported experimental results of multiple crack detection for long range inspections. Ditri and Rose [12] exploited the normal mode expansion technique to obtain the acoustic field distribution along a tube for an arbitrary applied surface traction.

Alleyne et al [13] reported the development of a dry piezoelectric transducer system for the excitation of axially symmetric modes in pipes. Alleyne et al [14] found experimentally that the strength of reflection of the L(0,2) mode from a notch in pipes is not altered much when it is taken as a through the thickness notch. Cawley et al [15] had studied the interaction of Lamb waves with defects in flat plates using plane strain models. Addison et al [16] presented Laser based ultrasound technique for the defect detection in tubes. They had implemented a laser array for generation of Lamb waves and identified suitable modes which can be used for the defect detection. Significant work on the guided waves was done by Rose et al [17]. In this work, the transducer were modified to isolate various modes of guided waves by using smaller phase velocity spectrum.

Alleyne et al [18] suggested the use of longitudinal mode in a non-dispersive region for the inspection of tubes over longer distances. They have used guided waves for the inspection of the pipes in chemical plants to detect the areas of corrosion, larger than 3tx3t and t/2 deep, where "t" is the wall thickness. The technique is to work on insulated pipes of 2 to 12 inches nominal diameter and at least 15m in length. Rose et al [19] discussed the mode selection criteria based on the acoustic field across the thickness of the waveguide, explaining why certain modes are sensitive to certain geometries of defects than others. Shin et al [20] used the non-axisymmetric modes for the faster and simpler inspection. The effect of the incident angle, frequency and the distance between the transducers was also elaborated in

3

the paper. Lowe et al [21] had proposed the theory of the mode conversion of guided waves in the tube inspection. The emphasis was on the conversion of the axisymmetric mode into non-axisymmetric modes due to the non-axisymmetric nature of defects. Rose et al [22] had proposed the idea of pipe comb transducer by using specific mode and frequency of guided waves. Ramakanth [23] had applied the concept of non-axisymmetric guided waves for the defect detection in tubes. He used three source locations at 120° apart at one end of the tube and monitored wave plots at these points. By processing these data, axial and angular locations of the defect were identified.

1.3   Present Work and Thesis Layout

In the present work, Finite Element Method is used for the simulation of the guided wave propagation in tubes. The emphasis is given on the mode conversion of the axisymmetric modes into non-axisymmetric modes. The axisymmetric mode is generated by applying small duration pulse all over the circumference at one end of the tube. From the displacement plots, the axial position of the crack is located.

Because of the non-axisymmetric nature of the defect, non-axisymmetric modes will also be present. The variation of longitudinal and flexural modes is plotted with respect to the crack size. These modes are used further for defect characterization of subsequent cases. This method is generalized for the circumferential nature of the cracks.

Chapter 2 deals with the theory of guided wave propagation in thin layers and in tubes. Mode selection criteria and mode conversion phenomenon are also explained which are used to carry out the subsequent analysis.

Chapter 3 explains the Finite Element modeling of wave propagation in tubes. FEM equations, displacement, strain, stress definitions are presented. In this dynamic formulation, lumped mass system and Newmark's technique of integration are explained. This FEM formulation is used to get the nodal displacements of the present problem in time domain.

Chapter 4 deals with the loading arrangement and imaging technique used in the present work. It also deals with the post processing methodology adapted to the FEM results, for the defect detection and characterization. The results of this analysis are given in the next chapter.

Chapter 5 gives the results and discussion of various cases. The methodology explained in the previous chapter is implemented and the results are presented.

Chapter 6 presents the conclusions of the present work and the scope for the future work.

Chapter 2

Guided Wave Propagation in Thin Walled Structures

2.1 Introduction

This Chapter gives the basics of guided wave propagation in thin layers. From classical elasticity theory, the general wave equations are formed. The theory is then specialized for the cylindrical structures such as tubes and rods. The frequency relation and the dispersion phenomenon are explained. At the end, the selection of modes for a particular application is discussed.

2.2 Guided Wave Propagation

The wave equation in linear elastic material can be derived from the classical elasticity theory [24]. The vector differential equation of motion in three dimension, for elastic isotropic medium is given by,

$$\mu \nabla^2 \underline{u_i} + (\lambda + \mu) \nabla \cdot (\nabla \cdot \underline{u_i}) = \rho \cdot \underline{\ddot{u}_i} \tag{2.1}$$

where, u_i : Displacement in x_i direction, $i = 1, 2, 3$

λ, μ : Lame's constants

ρ : Density of the material

∇ : $\frac{\partial}{\partial x_1} + \frac{\partial}{\partial x_2} + \frac{\partial}{\partial x_3}$

As it is difficult to solve these coupled equations directly, displacements are expressed in terms of the derivatives of the scalar potentials ϕ and vector potential $\underline{\psi}$. This is known as Helmholtz's decomposition, which gives,

$$\underline{u_i} = \nabla \cdot \phi + (\nabla \times \underline{\psi}) \qquad (2.2)$$

with an essential condition, $\nabla \cdot \underline{\psi} = 0$

The potentials, in turn, satisfy the uncoupled wave equations. For two dimensional case, with x_1 along the propagation direction and x_2 along the thickness direction, above equations are simplified to,

$$\frac{\partial^2 \phi}{\partial x_1^2} + \frac{\partial^2 \phi}{\partial x_2^2} = \frac{1}{C_l^2} \frac{\partial^2 \phi}{\partial t^2} \qquad (2.3)$$

$$\frac{\partial^2 \psi_3}{\partial x_1^2} + \frac{\partial^2 \psi_3}{\partial x_2^2} = \frac{1}{C_t^2} \frac{\partial^2 \psi_3}{\partial t^2} \qquad (2.4)$$

where, $C_l^2 = \frac{\lambda + 2\mu}{\rho}$ and $C_t^2 = \frac{\mu}{\rho}$

The potentials satisfying these equations represent the solution of the wave equation. As mentioned earlier, for the guided waves, these potentials are defined as functions of the thickness of the structure and propagating along the layer direction. Thus, the solution can be represented in the form,

$$\phi = \phi(x_2) \cdot e^{i(kx_1 - \omega t)} \qquad (2.5)$$

with $\phi(x_2) = A_1 sin(px_2) + A_2 cos(px_2)$

$$\psi_3 = \psi_3(x_2) \cdot e^{i(kx_1 - \omega t)} \qquad (2.6)$$

7

with $\psi_3(x_2) = B_1 sin(qx_2) + B_2 cos(qx_2)$

where, $p^2 = \frac{\omega^2}{C_l^2} - k^2$ and $q^2 = \frac{\omega^2}{C_t^2} - k^2$,

k being the wave number and A_1, A_2, B_1, B_2 are constants.

Substituting these solutions in Equation 2.2, displacements and then the stresses can be expressed as,

$$u_1 = ik\phi + \frac{\partial \psi_3}{\partial x_2} \tag{2.7}$$

$$u_2 = \frac{\partial \phi}{\partial x_2} - ik\psi_3 \tag{2.8}$$

$$\tau_{21} = \mu \left(2ik\frac{\partial \phi}{\partial x_2} + k^2\psi_3 + \frac{\partial^2 \psi_3}{\partial x_2^2} \right) \tag{2.9}$$

$$\tau_{22} = \lambda \left(-k^2\phi + \frac{\partial^2 \phi}{\partial x_2^2} \right) + 2\mu \left(\frac{\partial^2 \phi}{\partial x_2^2} - ik\frac{\partial \psi_3}{\partial x_2} \right) \tag{2.10}$$

Depending upon the nature of variables ϕ and ψ_3, the wave propagation in elastic medium can be split into two types of the systems, symmetric and anti-symmetric modes. The constants, A_1, A_2, B_1, and B_2 in the equations of ϕ and ψ_3 can be determined by applying the appropriate boundary conditions in terms of displacements or stresses. For the homogeneous system of the equations, the determinant of the coefficients must vanish, which yields the *frequency relation*, i. e., the equation relating the frequency ω to the wave number k.

For the stress free boundary conditions, the boundary conditions are $\tau_{21} = \tau_{22} = 0$, which yields the frequency relation,

Symmetric modes:

$$\frac{tan(qh)}{tan(ph)} = \frac{-4pqk^2}{(q^2 - k^2)^2} \tag{2.11}$$

Antisymmetric modes:

$$\frac{tan(qh)}{tan(ph)} = \frac{-(q^2 - k^2)^2}{4pqk^2} \tag{2.12}$$

8

These are well-known Rayleigh-Lamb frequency equations. The symmetric modes are known as longitudinal modes as the average displacement over the thickness is along the longitudinal direction. For the antisymmetric modes, the average displacement is in the transverse direction and these modes are generally termed as flexural modes. These are implicit transcendental equations relating the phase velocity and the frequency. These are satisfied by infinite number of real, imaginary or complex values of the phase velocity. The real solutions for a given frequency represent undamped propagating modes while the imaginary roots represent exponentially decaying modes which do not propagate.

2.3 Guided Wave Propagation in Tubes

Guided wave propagation in cylindrical coordinates (r, θ, z) is given by the displacement equations along axial, radial and circumferential directions. The governing equations are,

$$\nabla^2 u - \frac{u}{r^2} - \frac{2}{r^2}\frac{\partial v}{\partial \theta} + \frac{1}{1-2\nu}\frac{\partial \Delta}{\partial r} = \frac{1}{C_t^2}\frac{\partial^2 u}{\partial t^2} \tag{2.13}$$

$$\nabla^2 v - \frac{v}{r^2} + \frac{2}{r^2}\frac{\partial u}{\partial \theta} + \frac{1}{1-2\nu}\frac{1}{r}\frac{\partial \Delta}{\partial r} = \frac{1}{C_t^2}\frac{\partial^2 v}{\partial t^2} \tag{2.14}$$

$$\nabla^2 w + \frac{1}{1-2\nu}\frac{\partial \Delta}{\partial z} = \frac{1}{C_t^2}\frac{\partial^2 w}{\partial t^2} \tag{2.15}$$

where, $\nabla^2 = \frac{\partial^2}{\partial r^2} + \frac{1}{r}\frac{\partial}{\partial r} + \frac{1}{r^2}\frac{\partial^2}{\partial \theta^2} + \frac{\partial^2}{\partial z^2}$

and $\Delta = \frac{\partial u}{\partial r} + \frac{1}{r}\left(\frac{\partial v}{\partial \theta} + u\right) + \frac{\partial w}{\partial z}$

As explained earlier, these displacements are expressed in terms of the potentials to get the respective uncoupled wave equations, which are given as,

$$\nabla^2 \phi = \frac{1}{C_l^2}\frac{\partial^2 \phi}{\partial t^2} \tag{2.16}$$

9

$$\nabla^2 \upsilon_z = \frac{1}{C_t^2} \frac{\partial^2 \psi_z}{\partial t^2} \tag{2.17}$$

$$\nabla^2 \psi_r - \frac{\psi_r}{r^2} - \frac{2}{r^2} \frac{\partial \psi_\theta}{\partial \theta} = \frac{1}{C_t^2} \frac{\partial^2 \psi_r}{\partial t^2} \tag{2.18}$$

$$\nabla^2 \psi_\theta - \frac{\psi_\theta}{r^2} - \frac{2}{r^2} \frac{\partial \psi_r}{\partial \theta} = \frac{1}{C_t^2} \frac{\partial^2 \psi_\theta}{\partial t^2} \tag{2.19}$$

But in case of cylindrical coordinates, while the equations of only ϕ and υ_z are uncoupled, the equations of ψ_r and ψ_θ are coupled to each other. Therefore, it is difficult to solve this set of equations. The solutions are in terms of ordinary Bessel functions of r and θ and propagating along the axial direction, as given by the expressions,

$$\phi = A_1 J_n(pr) cos(n\theta) e^{i(kz-\omega t)} \tag{2.20}$$

$$\psi_z = B_1 J_n(qr) sin(n\theta) e^{i(kz-\omega t)} \tag{2.21}$$

$$\psi_r = C_1 J_{n+1}(qr) sin(n\theta) e^{i(kz-\omega t)} \tag{2.22}$$

$$\psi_\theta = -C_2 J_{n+1}(qr) cos(n\theta) e^{i(kz-\omega t)} \tag{2.23}$$

The constants A_1, B_1, C_1, C_2 in these solutions can be determined by applying appropriate boundary conditions. For the solution to exist, the determinant of the coefficients must vanish, which produces the frequency relation, in ω, k and n. This is a transcendental equation which is satisfied by infinite number of modes of phase velocity.

As seen from the form of the solutions, these infinite number of modes of propagation can be classified into two broad classes: axisymmetric and non-axisymmetric modes. Motions which are independent of θ and depend only on r and z directions are axisymmetric. These axisymmetric motions belong to torsional and longitudinal motions. In flexural

modes, the field has additional component in circumferential direction and therefore it is non-axisymmetric.

The tangential motion governs the pure torsional disturbance of the tube, the propagation velocity of which is $\sqrt{G/\rho}$. For longitudinal motion in tube, infinite number of modes satisfy the frequency relation. For a special case of $k = 0$, the phase velocity has a simple form of $(E/\rho(1 - \nu^2))^{1/2}$ which is generally termed as "thin plate velocity" [25]. For aluminum having Poisson's ratio of 0.33, the thin plate velocity is $5128.46 m/s$.

2.4 Mode Selection

For NDT, out of several modes available, a certain mode(s) is selected depending upon its sensitivity to the particular problem. The factors which govern the mode selection are excitability, penetration ability, mode isolation, and mode conversion.

For defects detection, the longitudinal modes are the most important ones from the practical point of view. The lowest torsional mode can be used when an undistorted pulse propagation is required. For the inspection of 20% through thickness crack, modes having larger displacement at the outer surface are chosen. For the "kissing bond" problem, modes with high in-plane displacements and shear forces are found to be sensitive.

2.5 Mode Conversion

As mentioned in this Chapter, there are two types of modes present in the tubes, axisymmetric and non-axisymmetric modes. Longitudinal and torsional modes are axisymmetric type while flexural modes are non-axisymmetric modes.

Even if only one mode is excited, depending upon the nature of defects, and the dispersion curve, various other modes (which are close to excited mode, on the dispersion curve) are also generated. The present analysis uses the longitudinal mode for the excitation as it is simple to implement in practice. Depending upon the nature of defects, other non-axisymmetric modes will be generated. The amplitudes of these converted modes, in turn,
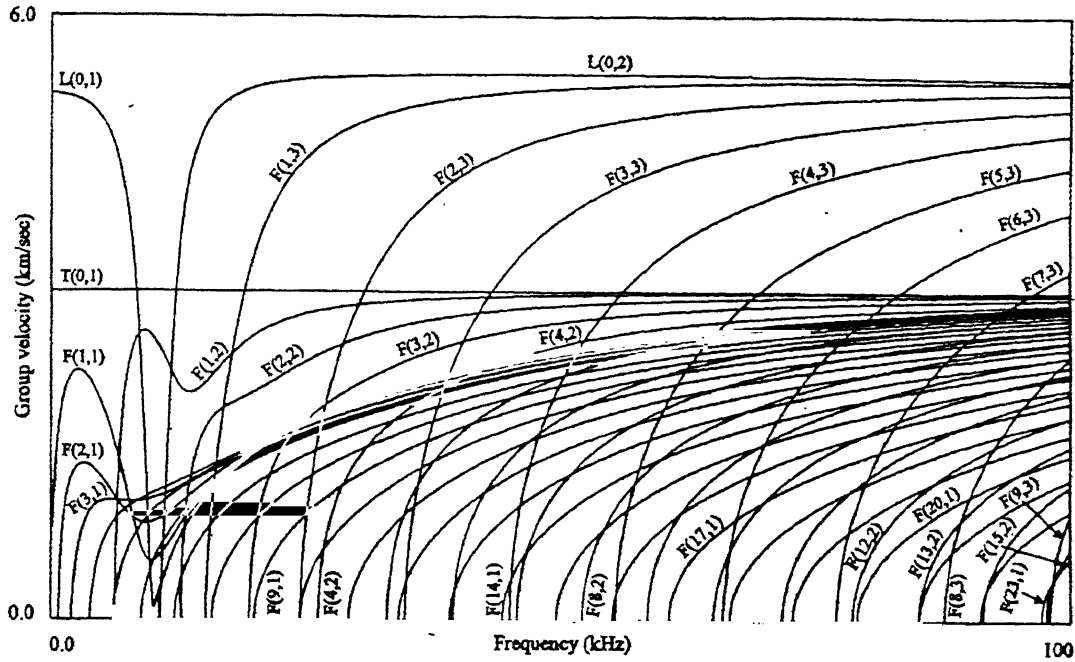
Figure 2.1: Group Velocity dispersion curves for 3" diameter steel pipe

have the information about the nature of defects.

Figure 2.1 shows various modes generated in a steel pipe of 3 inches diameter [20]. Longitudinal modes are represented by "L," flexural modes by "F," and torsional modes by "T." The first integer in the nomenclature indicates the harmonic order of circumferential variation while the second integer denotes the order of the higher modes of the respective type. Modes having zero as first integer are axially symmetric. The nature of F(1,3) mode is analogous to one half sinusoidal mode around the circumference and that of F(2,3) mode to two half sinusoidal modes around the circumference. The first flexural mode would be found in the axial displacements if the tube is subjected to gross bending [20].

Thus this Chapter discussed the basics of guided wave propagation in thin layers and tubes. This phenomenon is then modelled by finite element method in the next Chapter. After getting the finite element solution of the problem, the idea of mode conversion is used for the post processing and characterization of defects.

12

Chapter 3

FEM Formulation

3.1 Introduction

This Chapter explains the Finite Element Formulation of the wave propagation phenomenon in thin structures. The structure is approximated as an assembly of degenerated shell elements by Mindlin Plate Theory. FEM equations are formed by using virtual work principle. The integration of stiffness and force matrix is carried out by layered modeling of the structure to improve the accuracy.

Newmark's linear acceleration technique is employed for the time descretization. For simplicity, undamped system along with lumped masses and neglecting body forces is assumed for the present problem.

3.2 Mindlin Element Plate Theory

Classical shell theory involves several differential equations in terms of displacements which are complicated. They will take simple forms only if several simplifying approximations are made. Depending upon the assumptions and approximations made, various shell theories have been classified, such as, Dannial, Flügge, Vlasov, Kirchoff etc. Classical shell theory is concerned with thin shells, in which, transverse shear deformation is considered negligible. There are three approaches generally used in practice for the finite
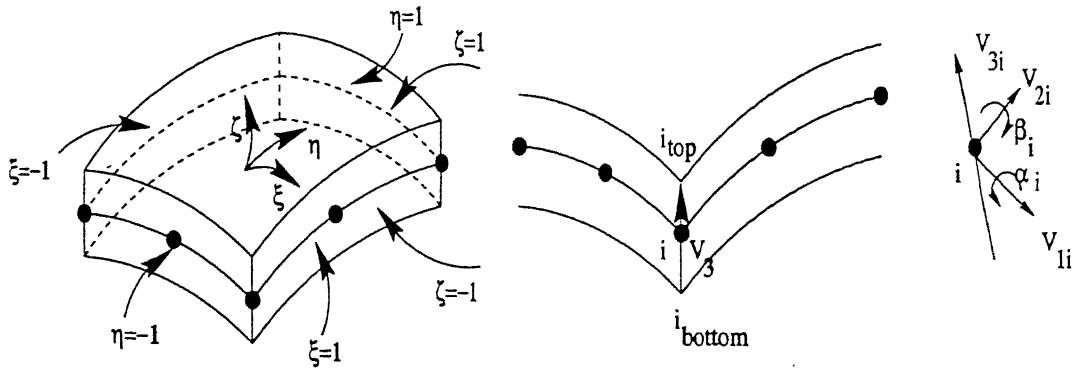
Figure 3.1: Element Geometry

element analysis of the shells.

The first is by approximating shells as an assembly of flat elements; the second is curved elements by classical shell theory and the third is Mindlin element theory. It is easy to formulate the shell as an assembly of flat elements but it looses the accuracy of the solution because of absence of bending continuity in individual elements. A curved shell element modeling improves the accuracy but at the cost of complexity in defining the geometry and additional nodal degrees of freedom. Mindlin type plate theory appeared to be a middle ground between the two, both in accuracy and ease in use. Mindlin elements are regarded as a special form of solid elements, made thin in one direction. The assumptions made in this analysis are:

1. The lateral deflection of the shell is small.

2. Normal to the mid plane of the shell before deformation remains straight but not necessarily normal to the mid plane after deformation.

3. The stress along the thickness direction is assumed to be zero, i. e., $\sigma_z = 0$.

3.3 FEM Formulation

Element Geometry

The geometry of a typical shell element is shown in Figure 3.1. ξ and η are two curvilinear coordinates in the middle plane of the shell. ζ is a linear coordinate normal to the middle

14

plane of the shell. These coordinates vary between $+1$ and -1 on the respective faces of the element and represent the local coordinate system.

As shown in Figure 3.1, the displacement at any point is expressed as,

$$
\left\{ \begin{array}{c} u \\ v \\ w \end{array} \right\} = \sum_{i=1}^{n} N_i(\xi, \eta) \frac{1+\zeta}{2} \left\{ \begin{array}{c} u_i \\ v_i \\ w_i \end{array} \right\}_{top} + \sum_{i=1}^{n} N_i(\xi, \eta) \frac{1-\zeta}{2} \left\{ \begin{array}{c} u_i \\ v_i \\ w_i \end{array} \right\}_{bottom}
\tag{3.1}
$$

where, n is number of nodes, $\{u_i\}_{top}$ and $\{u_i\}_{bottom}$ are displacements of top and bottom point of the ith node and $N_i(\xi, \eta)$ is the shape function at node i, taking unity value at i^{th} node and zero at other nodes. It is convenient to rewrite this definition by a vector connecting upper and lower points (length equals to the shell thickness) at the mid surface.

$$
\left\{ \begin{array}{c} u \\ v \\ w \end{array} \right\} = \sum_{i=1}^{n} N_i \left\{ \begin{array}{c} u_i \\ v_i \\ w_i \end{array} \right\}_{mid} + \sum_{i=1}^{n} N_i \frac{\zeta}{2} V_{3i}
$$

$$
or \quad \left\{ \begin{array}{c} u \\ v \\ w \end{array} \right\} = \sum_{i=1}^{n} N_i \left\{ \begin{array}{c} u_i \\ v_i \\ w_i \end{array} \right\}_{mid} + \sum_{i=1}^{n} N_i \frac{\zeta}{2} t_i v_{3i}
\tag{3.2}
$$

The above displacements can be expressed in terms of rotations α_i and β_i, such that they can clearly locate the exact position of the point. Therefore, five degrees of freedom per node defined to uniquely locate the position of the point.

$$
\left\{ \begin{array}{c} u \\ v \\ w \end{array} \right\} = \sum_{i=1}^{n} N_i \left\{ \begin{array}{c} u_i \\ v_i \\ w_i \end{array} \right\}_{mid} + \sum_{i=1}^{n} N_i \frac{\zeta}{2} t_i \lfloor v_{1i} - v_{2i} \rfloor \left\{ \begin{array}{c} \alpha_i \\ \beta_i \end{array} \right\}
$$

which can be written as,

$$
\left\{ \begin{array}{c} u \\ v \\ w \end{array} \right\} = \sum_{i=1}^{n} \left[\begin{array}{ccccc} N_i & 0 & 0 & \zeta t_i N_i v_{1i}/2 & -\zeta t_i N_i v_{2i}/2 \\ 0 & N_i & 0 & \zeta t_i N_i v_{1i}/2 & -\zeta t_i N_i v_{2i}/2 \\ 0 & 0 & N_i & \zeta t_i N_i v_{1i}/2 & -\zeta t_i N_i v_{2i}/2 \end{array} \right] \left\{ \begin{array}{c} u_i \\ v_i \\ w_i \\ \alpha_i \\ \beta_i \end{array} \right\} \tag{3.3}
$$

$$
or \ \{u\} = [N] \, \{u\}^{(e)} \tag{3.4}
$$

$$
where, \ [N] = \sum_{i=1}^{n} \left[\begin{array}{ccccc} N_i & 0 & 0 & \zeta t_i N_i v_{1i}/2 & -\zeta t_i N_i v_{2i}/2 \\ 0 & N_i & 0 & \zeta t_i N_i v_{1i}/2 & -\zeta t_i N_i v_{2i}/2 \\ 0 & 0 & N_i & \zeta t_i N_i v_{1i}/2 & -\zeta t_i N_i v_{2i}/2 \end{array} \right]
$$

Strain Vector

In the Mindlin element formulation, the strain in the thickness direction is taken negligible. Therefore, the strain vector is given as,

$$
\{\epsilon\} = \left\{ \begin{array}{c} \epsilon_x \\ \epsilon_y \\ \gamma_{xy} \\ \gamma_{yz} \\ \gamma_{zx} \end{array} \right\} = \left\{ \begin{array}{c} \partial u/\partial x \\ \partial v/\partial y \\ (\partial v/\partial x) + (\partial u/\partial y) \\ (\partial w/\partial y) + (\partial v/\partial z) \\ (\partial u/\partial z) + (\partial w/\partial x) \end{array} \right\}
$$

16

$$i.e., \{\epsilon\} = \begin{bmatrix} 1 & 0 & 0 & 0 & 0 & 0 & 0 & 0 & 0 \\ 0 & 0 & 0 & 0 & 1 & 0 & 0 & 0 & 0 \\ 0 & 1 & 0 & 1 & 0 & 0 & 0 & 0 & 0 \\ 0 & 0 & 0 & 0 & 0 & 1 & 0 & 1 & 0 \\ 0 & 0 & 1 & 0 & 0 & 0 & 1 & 0 & 0 \end{bmatrix} \begin{Bmatrix} u_{,x} \\ u_{,y} \\ u_{,z} \\ v_{,x} \\ \vdots \\ w_{,z} \end{Bmatrix} = [A_1]\{u_{,x}\} \qquad (3.5)$$

$$\{u_{,x}\} = \begin{bmatrix} [J]^{-1} & 0 & 0 \\ 0 & [J]^{-1} & 0 \\ 0 & 0 & [J]^{-1} \end{bmatrix} \begin{Bmatrix} u_{,\xi} \\ u_{,\eta} \\ u_{,\zeta} \\ v_{,\xi} \\ \vdots \\ w_{,\zeta} \end{Bmatrix} = [A_2]\{u_{,\xi}\} \qquad (3.6)$$

where, $[J]^{-1}$ is the inverse of the 3×3 Jacobian matrix $[J]$.

$$\{u_{,\xi}\} = \sum_{i=1}^{n} \begin{bmatrix} N_{i,\xi} & 0 & 0 & \zeta N_{i,\xi}t_i v_{1i}/2 & -\zeta N_{i,\xi}t_i v_{2i}/2 \\ N_{i,\eta} & 0 & 0 & \zeta N_{i,\eta}t_i v_{1i}/2 & -\zeta N_{i,\eta}t_i v_{2i}/2 \\ 0 & 0 & 0 & N_i t_i v_{1i}/2 & -N_i t_i v_{2i}/2 \\ 0 & N_{i,\xi} & 0 & \zeta N_{i,\xi}t_i v_{1i}/2 & -\zeta N_{i,\xi}t_i v_{2i}/2 \\ \vdots & \vdots & \vdots & \vdots & \vdots \\ 0 & 0 & 0 & N_i t_i v_{1i}/2 & -N_i t_i v_{2i}/2 \end{bmatrix} \{u\}^{(e)} = [A_3]\{u\}^{(e)}$$

$$(3.7)$$

Substituting Equations 3.6 and 3.7 in Equation 3.5,

$$\{\epsilon\} = [A_1][A_2][A_3]\{u\}^{(e)}$$

$$\{\epsilon\} = [B]\{u\}^{(e)} \qquad (3.8)$$

17

where, $[B] = [A_1][A_2][A_3]$, $[A_1]$, $[A_2]$, and $[A_3]$ are as defined in Equations 3.5, 3.6, and 3.7 respectively.

Stress Vector

Depending upon the assumptions made earlier in the Mindlin plate theory, stress along the normal to the middle plane is considered as zero, i. e., $\sigma_z = 0$. Therefore the stress vector is expressed in terms of strains as,

$$\{\sigma\} = \begin{Bmatrix} \sigma_x \\ \sigma_y \\ \tau_{xy} \\ \tau_{xz} \\ \tau_{yz} \end{Bmatrix} = \frac{E}{1-\nu^2} \begin{bmatrix} 1 & \nu & 0 & 0 & 0 \\ \nu & 1 & 0 & 0 & 0 \\ 0 & 0 & \frac{1-\nu}{2} & 0 & 0 \\ 0 & 0 & 0 & \frac{1-\nu}{2k_f} & 0 \\ 0 & 0 & 0 & 0 & \frac{1-\nu}{2k_f} \end{bmatrix} \{\epsilon\}$$

$$\{\sigma\} = [D]\{\epsilon\} = [D][B]\{u\}^{(e)} \tag{3.9}$$

where, $[D]$: Material property matrix

k_f : Factor introduced to improve strain approximation

FEM Equation

Equations that govern the dynamic response of a structure is derived by using the virtual work principle involving work of external forces, internal, inertial and viscous forces for any small admissible motion. For a single element, this work balance becomes,

$$\int_{\Omega} \{\delta\epsilon\}^T \cdot \{\sigma\}\, dV + \int_{\Omega} \{\delta u\}^T \rho\, \{\ddot{u}\}\, dV + \int_{\Omega} \{\delta u\}^T k_d\, \{\dot{u}\}\, dV$$

$$= \int_{\Omega} \{\delta u\}^T \cdot \{P_B\}^{(e)}\, dV + \int_{\Gamma_\sigma} \{\delta u\}^T \cdot \{P_s\}^{(e)}\, ds \tag{3.10}$$

18

where, $\{\delta u\}, \{\delta\epsilon\}$: Small displacements and corresponding strains

$\{\dot{u}\} \{\ddot{u}\}$: Velocity and accelerations

ρ : Material density

k_d : Damping coefficient

$\{P_B\}$: Body forces

$\{P_S\}$: Surface traction

Γ_σ : Surface traction boundary

The present analysis is made for an undamped system and neglecting body forces. The stresses, strains and displacements are expressed in terms of nodal variables as given in Equations 3.4, 3.8 and 3.9. This substitution gives,

$$\{\delta u\}^T \left[\int_\Omega [B]^T [D] [B] \, dV \, \{u\}^{(e)} + \int_\Omega \rho [N]^T [N] \, dV \, \{\ddot{u}\}^{(e)} - \int_{\Gamma_\sigma} [N]^T \{P_S\} \, dV \right] = 0$$

$$(3.11)$$

Since $\{\delta u\}$ is taken arbitrary, satisfying kinematic conditions, the equation can be written as,

$$\int_\Omega [B]^T [D] [B] |J| \, d\xi d\eta d\zeta \, \{u\}^{(e)} + \int_\Omega \rho [N]^T [N] |J| \, d\xi d\eta d\zeta \, \{\ddot{u}\}^{(e)}$$

$$= \int_{\Gamma_\sigma} [N]^T \{P_S\}^{(e)} |J| \, d\xi d\eta$$

It can be written in a compact form as,

$$[K]^{(e)} \{u\}^{(e)} + [M]^{(e)} \{\ddot{u}\}^{(e)} = \{F\}^{(e)}$$

$$(3.12)$$

where, Elemental stiffness matrix, $[K]^{(e)} = \int_\Omega [B]^T [D] [B] |J| \, d\xi d\eta d\zeta$

Elemental mass matrix, $[M]^{(e)} = \int_\Omega \rho [N]^T [N] |J| \, d\xi d\eta d\zeta$

Elemental force matrix, $\{F\}^{(e)} = \int_{\Gamma_\sigma} [N]^T \{P_S\}^{(e)} |J| \, d\xi d\eta$

19

After assembling, these elemental equations can be written in global form as,

$$[K]\{u\} + [M]\{\ddot{u}\} = \{F\} \qquad (3.13)$$

where, Global stiffness matrix, $[K] = \sum [K]^{(e)}$

Global mass matrix, $[M] = \sum [M]^{(e)}$

Global force vector, $\{F\} = \sum \{F\}^{(e)}$

Layered Model

If the shell is built up of different materials, such that the material properties are discontinuous functions of ζ, an appropriate integration through the thickness has to be carried out. Here layered approach is employed, wherein, a mid-point integration scheme is adapted for each layer. The stress components of the layer are computed at the mid-points and are assumed to be constant over the layer thickness. The specification of the layer thickness in terms of curvilinear coordinate, ζ, permits the variation of layer thickness.

The normal forces and bending moments are obtained by integrating the corresponding stress component with respect to the thickness coordinate.

$$\sigma_{xx} = \int_{-h/2}^{h/2} \sigma_x dz = \frac{h}{2} \sum_{i=1}^{p} \sigma_x^i \Delta \zeta^i$$

$$M_x = \int_{-h/2}^{h/2} \sigma_x z dz = -\frac{h^2}{4} \sum_{i=1}^{p} \sigma_x^i \zeta^i \Delta \zeta^i$$

where p is the number of layers and h is the layer thickness.

In the present code, matrix $[B]$ is calculated at the mid-surface of each layer. The element stiffness matrix $[K]^{(e)}$ and force matrix $\{F\}^{(e)}$ are thus defined as,

$$[K]^{(e)} = \int \int_{-1}^{+1} [B]^T [D] [B] |J| d\zeta dA \qquad (3.14)$$

$$\{F\}^{(e)} = \int \int_{-1}^{+1} [B]^T \{\sigma\}^{(e)} |J| d\zeta dA \qquad (3.15)$$

where, $\int ...dA = \int_{-1}^{+1} \int_{-1}^{+1} ...d\xi d\eta$

This process of integration in the thickness direction is computationally more expensive, but is more appropriate for thick shells and variable thickness problems.

3.4 Solution Procedure

From finite element formulation, the energy balance for any element of the system can be written as,

$$[K] \{u\} + [M] \{\ddot{u}\} = \{F\}$$

This equation represents a system of coupled, second order, ordinary differential equations. Although the displacements are discrete functions of space, they are continuous functions of time. The shape functions $[N]$ are same as used for the displacement field interpolation in Equation 3.4. First three columns in the shape functions account for the translational inertia while the last two columns correspond to the rotational moments of inertia of the shell. The present analysis takes into consideration rotational inertia as well.

The mass and stiffness matrices so obtained, are known as *consistent matrices*, which are symmetric and positive definite. A much simpler analysis can be performed by *lumping* the mass only at the node points. This method of *mass lumping* produces diagonal mass matrix, the sum of diagonal elements being equal to the mass of the element. The Figure 3.2 shows the consistent and lumped masses for 8-noded isoparametric element considering the rotational moment of inertia.

There are two methods of finite difference available to solve the ordinary differential equations, *implicit* and *explicit* methods. In the explicit finite difference method, such as central difference method, the solution at time $t + \Delta t$ is calculated using the equilibrium condition at time t. Where as in implicit methods, such as, Houbolt, Wilson and Newmark
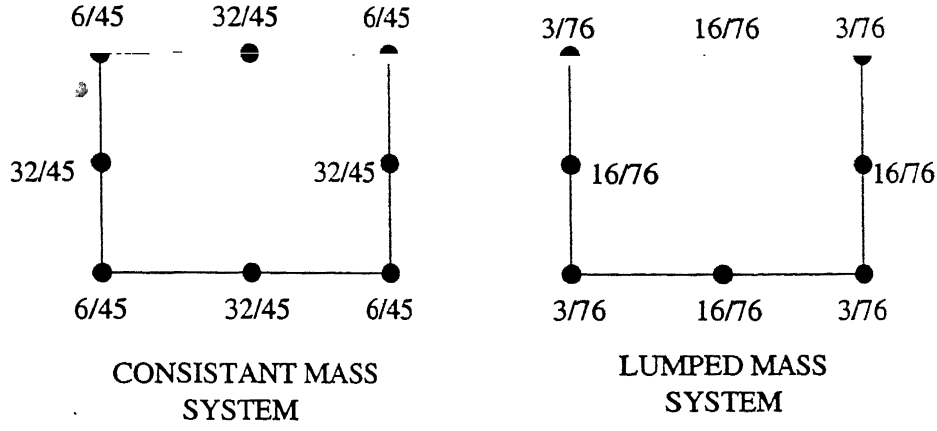
Figure 3.2: Distribution of mass over the element

methods, equilibrium conditions at time $t + \Delta t$ are used. Since, in explicit method, the time step is incremented step-by-step, a special starting procedure has to be employed using initial values. It does not require the factorization of the effective stiffness matrix in each increment. However, in all implicit methods, the effective stiffness matrix has to be factorized in each iteration. In the present analysis, Newmark's method has been employed for the dynamic analysis.

3.4.1 Newmark's method of Integration

Newmark's method is an extension of the linear acceleration method, in which, a linear variation of the acceleration is assumed from time t to $t + \Delta t$. The velocity and acceleration are approximated in terms of displacements as,

$$^{t+\Delta t}\dot{U} = {}^{t}\dot{U} + \left[(1 - \delta)\ {}^{t}\ddot{U} + \delta\ {}^{t+\Delta t}\ddot{U}\right]\Delta t \tag{3.16}$$

$$^{t+\Delta t}U = {}^{t}U + {}^{t}\dot{U}\Delta t + \left[\left(\frac{1}{2} - \alpha\right)\ {}^{t}\ddot{U} + \alpha\ {}^{t+\Delta t}\ddot{U}\right]\Delta t^{2} \tag{3.17}$$

where α and δ are parameters chosen suitability to have accuracy and stability. Usually, α and δ are taken as 0.25 and 0.5 respectively to get unconditional stability. As mentioned earlier, the equilibrium at time $t + \Delta t$ is considered along with these approximations. Solving Equations 3.16 and 3.17, we get expressions for $^{t+\Delta t}U$ and $^{t+\Delta t}\ddot{U}$, in terms of the

unknown displacement $^{t+\Delta t}U$. These are then substituted in the following equation to solve for $^{t+\Delta t}U$.

$$[M]^{t+\Delta t}\left\{\ddot{U}\right\} + [K]^{t+\Delta t}\{U\} = {}^{t+\Delta t}\{F\} \qquad (3.18)$$

The steps can be summarized as follows:

1. Form the global stiffness matrix $[K]$, and mass matrix $[M]$.

2. Initialize ^{0}U, $^{0}\dot{U}$, $^{0}\ddot{U}$.

3. Select time step Δt and calculate integration constants:

   $a_0 = \frac{1}{\alpha \Delta t^2}$; $a_1 = \frac{\delta}{\alpha \Delta t}$; $a_2 = \frac{1}{\alpha \Delta t}$; $a_3 = \frac{1}{2\alpha} - 1$; $a_4 = \frac{\delta}{\alpha} - 1$;

   $a_5 = \frac{\Delta t}{2}\left(\frac{\delta}{\alpha} - 2\right)$; $a_6 = \Delta t(1 - \delta)$; $a_7 = \delta \Delta t$

4. Form effective stiffness, $[K'] = [K] + a_0[M]$

5. For each time step:

   (i) Calculate effective load at $t + \Delta t$:

   $$^{t+\Delta t}\{F'\} = {}^{t+\Delta t}\{F\} + [M]\left(a_0^t\{U\} + a_2^t\left\{\dot{U}\right\} + a_3^t\left\{\ddot{U}\right\}\right)$$

   (ii) Solve for displacement at time $t + \Delta t$ by $[K']^{t+\Delta t}\{U\} = {}^{t+\Delta t}\{F'\}$.

   (iii) Calculate acceleration and velocity at time $t + \Delta t$:

   $$^{t+\Delta t}\ddot{U} = a_0\left(^{t+\Delta t}U - {}^{t}U\right) - a_2^t\dot{U} - a_3^t\ddot{U}$$

   $$^{t+\Delta t}\dot{U} = {}^{t}\dot{U} + a_6^t\ddot{U} + a_7^{t+\Delta t}\ddot{U}$$

3.4.2 Remarks on stability

In the dynamic modeling of the finite elements, it is very important to look for the stability and accuracy of the solution. This is because of the simultaneous descretization in space and time domain. There are some guidelines in this aspect which are listed below:

23

- In finite element descretization with *lumped masses*, the maximum frequency (for the stress wave propagation) is taken as,

$$(\omega_{max})_e = \frac{2c}{L}$$

where, L : Effective element length, or smallest length along the propagation direction

  c : Speed at which the wave travels in the structure, usually taken as the dilatation or acoustic speed, equal to $\sqrt{E/\rho}$.

- The time step chosen for the finite difference should not be too large from accuracy point of view. Also it should not be too small, otherwise the computations become expensive. Generally, a condition, known as *CFL condition* is followed.

$$\Delta t \leq \frac{2}{\omega_{max}} = \frac{L}{c}$$

The physical interpretation of this condition is that Δt must be small enough so that the stress wave does not propagate across more than one element per time step. A normal practice is to take at least 4-5 steps to cross one element.

- Also, another important parameter is the finite element descretization of the domain. Depending upon the applied load frequency (i. e. the wavelength), the mesh size is chosen such that there are at least 5-6 elements over the wavelength.

Thus, this Chapter dealt with the Finite Element Formulation of the wave propagation phenomenon in shells. The geometry is approximated in degenerated shell elements by Mindlin plate theory. The time descretization is carried out by linear acceleration implicit method. Finite element results gives the nodal displacements on the time domain. These displacements are further processed for defect detection and characterization. The next Chapter deals with the post processing methodology adopted for this purpose.

Chapter 4

Data Analysis and Crack Detection

4.1 Introduction

This Chapter describes the loading and monitoring systems used for the present work. It discusses the post processing methodology adopted for the defect detection and characterization. The method is generalized for the cracks having circumferential nature as these are commonly occur in practice.

4.2 Loading System

The arrangement used for the loading is shown in Figure 4.1. Short duration axially symmetric pulse is applied all over the circumference of the tube, thereby generating $L(0,2)$ mode. Loading points on the circumference resembles to the number of transducers on the periphery.

The advantage of using longitudinal mode is that it has predominant motion in axial direction which is easy to detect by strain gauges. Practically, it is difficult to create only one particular mode, as there are several components along with the applied one. For the applied $L(0,2)$ mode, it is possible that $L(0,1)$ mode will also be created. But by using certain filters, it is possible to separate the unwanted $L(0,1)$ mode from the $L(0,2)$ mode. From the dispersion curve, given in Figure 2.1, it is observed that $L(0,2)$ mode has the
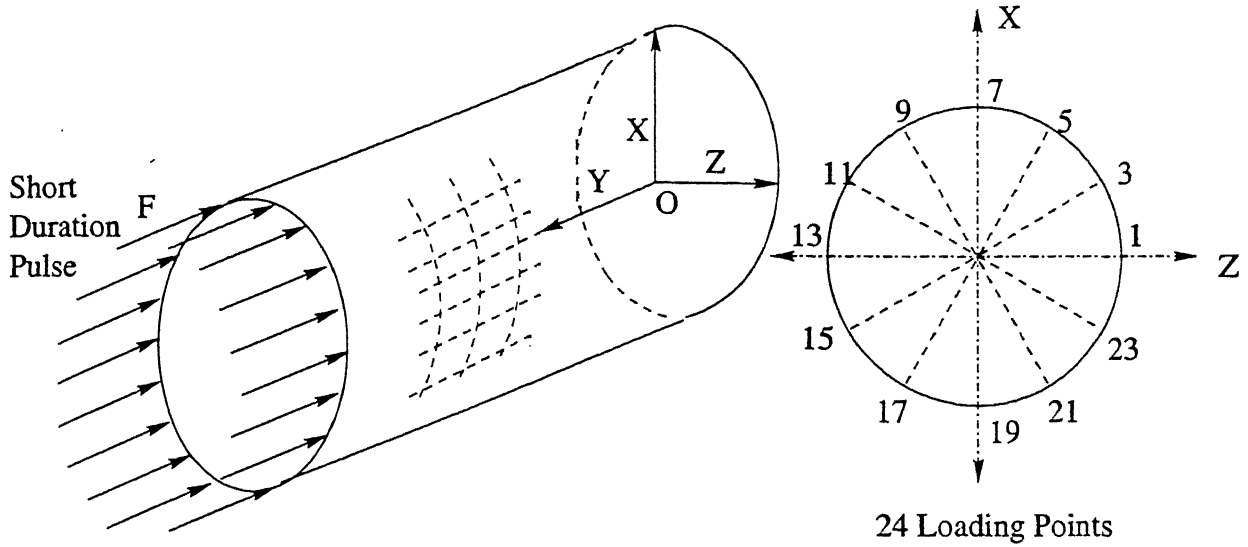
Figure 4.1: Loading arrangement

highest speed among all longitudinal modes and is also of non-dispersive nature. Therefore, it can be used for long range monitoring applications. Also, there are few neighbouring modes *(F(1,3)* and *F(2,3))* to *L(0,2)* which means that the mode conversion will not create much complications. These *F(1,3)* and *F(2,3)* modes contain important information about the nature of the defects and are easy to detect.

4.3 Imaging Techniques

Analysis of the flaw information is very crucial part in NDE process. Several presentation techniques are available to present the information. These can be classified as A-Scan, B-Scan and C-scan techniques. The choice of a particular one is made depending upon the type of information required, ease of measurement and suitability for a given geometry of the part.

In the A-Scan technique, signals are sent and received at one point. The reflected wave is recorded in time domain and post processing is performed on the recorded data to get the location and size of the defect. B-scan representation gives the profile of the part at some constant thickness. The probe is moved along a line, simultaneously recording the reflections. The reflected amplitudes are plotted depending upon the depth of the defect.

By using multiple and angular B-Scans, 3-D pictures of the defect can be plotted. C-Scan display gives the plan view of the part along with the defected region, the contours/colours of the region indicating the depth of the defect. It gives good pictorial information about the location and severity of the defect.

4.4 Signal Processing and Crack Detection

In the present analysis, the axial displacements are recorded at transmitter locations as a function of time. Initially, for a defect free specimen, the input signal is applied at one end and the displacement variation is recored. The observation is made till the input pulse is reflected from the far end of the tube. This data for a defect free specimen is used to calculate the longitudinal wave speed in the tube and as a reference for the future inspection.

Loading is then applied on the specimen with crack and similar displacement variations are recorded. All these time domain informations are converted into frequency domain by applying Fast Fourier Transform (FFT). This gives amplitudes of various frequencies. As discussed in the previous Chapters, a good choice of the amplitude is made. It is suggested to select the amplitude of higher frequencies than the applied one but not more than the maximum frequency, which is compatible with the meshing used. These amplitudes are processed further to get the required information about the defects in the tube, as discussed in the foregoing Sections.

4.4.1 Circumferential Crack

A through thickness crack is modelled in FEM by disconnecting the adjacent edges of neighbouring elements. Axial position of the crack can be easily located from the displacement variation. In this procedure, angular position of the crack is first located.

1. Determination of Angular Position

    An axially symmetric $L(0,2)$ mode pulse is applied at a few number of equiangular circumferential points at one end of the tube. The reflected wave in axial direction is

recorded for a time duration till the wave arrives from the far end of the tube. This time domain information is then converted into frequency domain by applying Fast Fourier Transform (FFT).

Proper choice is made in selecting the frequency to observe the amplitudes. In the present work, the amplitudes of the maximum frequency which is compatible to the meshing used are observed.

These amplitudes are then plotted on the circumference of the tube. For the circumferential nature of the defect, the variation will be symmetric about a certain point. The crack is supposed to be situated about the point having minimum displacement.

2. Determination of Axial Position

An axially symmetric load pulse (similar to the one above) is applied on the tube with crack. Initially, angular position of the crack is located, which will corresponds to a point (on the circumference) having minimum displacement. The displacement variation at that angular location contains the reflection from the crack. The axial location is determined from the time of arrival of the reflecting signal and the longitudinal wave speed.

3. Size of the crack

The reflected wave contains several modes. As discussed in the earlier topics, for the applied $L(0,2)$ mode pulse, flexural modes $F(1,2)$ and $F(1,3)$ will be of prime importance. Also the wave will have some component of $L(0,1)$ mode, but it is not taken into account. For very accurate results, by applying some filters, these unwanted modes can be eliminated.

Reflected waves are recorded for a crack free model. Axial displacements of all the transmitting points are added together. This is used as a reference value to get the magnitudes of the longitudinal modes of the subsequent models having cracks.

Reflections are collected in the same manner for a specimen with a crack. These

28

are added and the reference signal (from crack free model) is subtracted (this will take care of the rigid body motion, if any). This addition will give the longitudinal mode for the corresponding crack.

$L(0,2) \, Amplitude = a_1 + a_2 + \ldots\ldots + a_n$

where, n : Number of points used on the circumference

$a_1, a_2, \ldots.a_n$: Amplitudes on the corresponding points

For flexural modes $F(1,3)$ and $F(2,3)$, first integer (in the nomenclature) gives the circumferential order. To get the amplitudes of these modes, the individual signals are added to each wave data with a phase delay of $N\theta$, where N corresponds to the circumferential order and θ is the crack angle.

$F(1,3) \, Amplitude = a_1 sin\theta_1 + a_2 sin\theta_2 + \ldots\ldots + a_n sin\theta_n$

$F(2,3) \, Amplitude = a_1 sin2\theta_1 + a_2 sin2\theta_2 + \ldots\ldots + a_n sin2\theta_n$

These additions were plotted with respect to the crack size, around the circumference. The amplitudes of these modes reveal important information about the nature and size of the crack.

4.4.2   Cracks with angular orientation

The above methodology is suitable only for circumferential cracks. For the cracks at different orientation, it is difficult to predict the angular position and the magnitudes of the converted modes. The plot of the axial displacement on the circumference will not be symmetrical about any point. Therefore the addition of the waves will not give good characterization.

All the individual waves in the axial direction are collected and plotted on the circumference. The asymmetric nature will show that the crack is not of circumferential nature.

Thus, this Chapter presented the steps for crack detection and crack characterization by using mode conversion criteria. All these steps are followed after the FEM solution and the results are presented in the next Chapter.

Chapter 5

Results And Discussion

This Chapter deals with the results and discussion of the crack detection using the method presented in earlier Chapters. The code is validated and the output is compared with the standard results. As per the method discussed in Section 4.4, the modes generated due to the circumferential crack are extracted and plotted. The results are analyzed to characterize the cracks.

5.1 Validation of the Code

A Finite Element Code for the Wave Propagation in plates and shells (Ramakanth [23]) is modified to take into consideration the rotary moment of inertia of the shell.

The code is used to obtain the wave propagation results for a case of an aluminum tube (Elastic modulus $69.0 GPa$, Shear modulus $26.4 GPa$ and density $1800 Kg/m^3$). The tube of length $350mm$, $18.86mm$ outer diameter and $1.2mm$ shell thickness is descretized into $960(24 \times 40)$ elements. The loading arrangement is shown in Figure 5.1. A short duration loading pulse in axial and tangential direction is applied at three locations which are 120° apart circumferentially. The frequency used is $0.1 MHz$ and the duration of the pulse is $10\mu s$. Reflected waves are recorded at these points and compared well with the results of Ramakanth [23]. The displacement variation at one of the loading points is shown in Figure 5.2. The oscillations are found to be smaller than the previous results (Ramakanth [23]),

30

which may be because of the added rotary moments of inertia.

5.2 Characterization of Circumferential Cracks

In the present work, various methods to characterize the cracks; i. e., its angular location, axial location and size of the crack have been discussed. Several cases of cracks are analyzed.

5.2.1 Geometry and Material Data

The geometry of the specimen, material properties, mesh details of the tube and the input pulse variation used for the present analysis are given below.

Material Properties

A tube of outer diameter $18.86mm$ and $1.2mm$ thick is used in the present analysis. The length of the tube is $350mm$. The material used in the present work is isotropic, elastic aluminum, the properties of which are listed here.

- Density, ρ : $2700Kg/m^3$

- Elastic Modulus, E : $70.9GPa$

- Poisson's ratio, ν : 0.33

- Shear Modulus, G : $26.4GPa$

- Longitudinal wave speed, C_l : $6194.4m/s$

- Shear wave speed, C_s : $3126.9m/s$

- Dilatation speed, C : $5124.7m/s$

Mesh Details

The tube is analyzed using finite elements by Mindlin shell theory. For dynamic analysis, it is suggested to use only linear elements [27], but to take care of the curvature, isoparametric quadratic elements are used.

- Type of elements: $8 - noded\ isoparametric\ element$

31

- Nodal degrees of freedom: 5 (*translations along x, y, z and rotations about x and y*)

- No. of elements: 960 (24 *along circumferential and* 40 *along axial direction*)

- Number of nodes: 2928

- Number of layers: 10

- Elemental length along the propagation direction, L : $8.75mm$

- Maximum frequency that can be modelled, $C/\pi L$: $1.864 \times 10^5 Hz$

Input Pulse

A short duration compressive pulse of the form $(1 - cos(\omega t))$ is used all along the circumference on 24 equiangular points. One complete cycle of the pulse is applied for the duration of $25\mu s$ in 50 time steps. The frequency used is well below the maximum possible frequency, compatible with the meshing. Figure 5.3 shows the input pulse variation.

- Force magnitude: $15KN$ *Compressive*

- Applied frequency, f : $40KHz$

- Pulse duration: $25\mu s$

- Time step, Δt : $0.5\mu s$

5.2.2   Crack Free Model

A crack free specimen is shown in Figure 5.4. The pulse is applied for a duration of $25\mu s$ and the displacements are monitored for $250\mu s$. Snapshots of axial displacements are shown in Figure 5.5 and Figure 5.6 at a few time instants. Figure 5.7 shows the displacement variation at one of the loading point. These variations will be same at all the points on the circumference for a crack free specimen. These plots are used as reference for the further cases, with cracks.

From this variation, it seems that the first $20-25\mu s$ correspond to the input pulse. Once the input pulse is completed, the displacement after few time step attenuates and converges to a certain displacement. This displacement corresponds to the rigid body motion. In the

present case, as the input is applied all along the circumference, the effect of attenuation in not reflected in the plot. After $120\mu s$, there is significant change in the amplitude. This reveals that the reflected pulse from the rear end is reaching the transmitting point. The arrival time of the reflected wave gives the longitudinal velocity of $5147.05m/s$ which is very close to the dilation speed $5124.7m/s$ of the material used.

5.2.3 Determination of Angular Location

The reflected waves are collected at all the points on the circumference. The displacement variations are observed till the wave is reflected to the transmitting point. Fast Fourier Transform (FFT) is applied to these time domain data to get the frequency domain amplitudes. The nature of these frequency domain amplitudes at few points are shown in Figure 5.8. These show that the amplitudes at lower frequencies are greater than that at higher frequencies. Using these amplitudes, angular locations for two cases of cracks are determined.

Case 1: Circumferential Crack at $175mm$ and 135°

Geometry of the circumferential crack is shown in Figure 5.9. The crack size corresponds to an angle of 90°, i. e., starting from point 7 to point 13. The crack is situated at $175mm$ from the front end and at 135° from point 1.

The amplitudes of $183.5KHz$ component (near the maximum frequency compatible to the meshing) are collected and plotted in Figure 5.10. From the figure, minimum displacement is at point 10 and the variation is also symmetric about it. Therefore, the center of the crack is at point 10, i. e., at about 135° from point 1.

Case 2: Circumferential Crack at $262.5mm$ and 225°

Geometry of the circumferential crack is shown in Figure 5.11. The crack size corresponds to an angle of 90°, i. e., starting from point 13 to point 19. The crack is situated at $262.5mm$ from the front end and at 225° from point 1.

The amplitudes at $183.5KHz$ component (near the maximum frequency compatible to

the meshing) are collected and plotted in Figure 5.12. From the figure, minimum displacement is at point 16 and the variation is also symmetric about it. Therefore, the center of the crack is at point 16, i. e., at about 225° from point 1.

5.2.4 Determination of Axial Location

As explained in Section 4.4.1, for locating the axial position of the crack, angular location of the center of the crack is determined initially. Axial displacement variation at the corresponding angular location is observed to get the axial location of the crack.

Case 1: Circumferential Crack at $175mm$ and 135°

As given in Section 5.2.3, the angular orientation for this crack is determined first. The center of the crack is at point 10, i. e., 135° from point 1. Displacement variation of point 10 is shown in Figure 5.13. It can be observed from the plot that the reflection from the crack starts at about $68\mu s$. From the velocity of the wave $(5147.05m/s)$, the axial location of the crack is at $175mm$ from the front end.

Case 2: Circumferential Crack at $262.5mm$ and 225°

As given in Section 5.2.3, the angular orientation for this crack is determined. The center of the crack is at point 16, i. e., 225° from point 1. Displacement variation of point 16 is shown in Figure 5.14. It can be observed from the plot that the reflection from the crack starts at about $105\mu s$. From the velocity of the wave $(5147.05m/s)$, the axial location of the crack is at $270mm$ from the front end.

5.2.5 Determination of Crack Size

To determine the size of the crack, reference wave data for various cracks at $175mm$ of sizes 0° to 360° of the circumference are to be analyzed. Each time the amplitudes were collected on the frequency domain. These amplitudes are then added to get the magnitudes of the respective modes. As explained in Section 4.4.1, the amplitudes are simply added

34

all over the circumference to get the magnitude of the $L(0,2)$ mode. For flexural modes, a phase delay of $N\theta$ is added to each wave data before summing up, where θ is the crack angle and N is the circumferential order.

By this addition method, amplitudes of various modes *L(0,2)*, *F(1,3)* and *F(2,3)* are determined and plotted with respect to the crack size. These individual modes are shown in Figure 5.15, 5.16 and 5.17 respectively. The longitudinal mode seems to be varying linearly with respect to the crack size. The flexural modes are varying sinusoidally around the circumference. *F(1,3)* mode completes one half sine curve over the circumference while *F(2,3)* mode has two half sine curves. These modes are used as reference modes for further cases.

Case 1:Circumferential crack at $175mm$ starting from 90° to 135°

Geometry of the crack is shown in Figure 5.9. As given in Section 5.2.3 and 5.2.4, angular and axial location for this crack are determined. It is found that the crack is situated around point 10, i. e., at 225° from point 1. Axial displacement variation of point 10 gives the axial position of the crack at $175mm$ from the front end. Then, amplitudes on the frequency domain are added together to get the magnitude of the longitudinal mode.

The magnitude of the *L(0,2)* mode is found to be 8.508×10^{-5}. From the *L(0,2)* mode, already plotted in Figure 5.15, the crack angle is found to be in between 60° and 120°. After locating this amplitude accurately on the *L(0,2)* mode, the size is taken as 90°. With this angle then, magnitudes of the other modes are calculated.

$$F(1,3) \ magnitude = 1.827 \times 10^{-5}$$

$$F(2,3) \ magnitude = 8.256 \times 10^{-5}$$

From Figure 5.16 and 5.17, it can be observed that these magnitudes correspond to a crack of 95° or 85° which agrees well with the actual size of the crack, 90°.

35

Discussion on the modes

From practical point of view, $L(0,2)$ mode is very much suitable for the crack detection. The nature of the mode is almost non-dispersive. It can be used for long range inspection. Also, the maximum phase velocity of the mode enable the effective inspection.

The variation of the longitudinal mode is linear with respect to the size of the crack, around the circumference. Therefore, to some extent, the amplitude of the longitudinal mode gives the size of the crack. And the flexural modes have the shape of half sine curves around the circumference with respective orders. For very small cracks, or for full circumferential cracks, the magnitudes of the flexural modes are almost zero. This logic can be extended to the cracks having axisymmetric nature. Thus, if the crack spread all over the circumference (as in case of joints and welds), then flexural modes will not be suitable for the inspection.

If the crack in the pipe consists of both axisymmetric as well as non-axisymmetric types, then the longitudinal mode can not differentiate between the two. In such cases, flexural modes are enough to detect the crack.

From $L(0,2)$ and $F(1,3)$ modes, it seems that, for very small cracks, their nature is almost identical to each other. Therefore, in such cases, there is another option of using flexural modes instead of longitudinal, if the conditions demand so.

The major difficulty of the signal processing is the addition of the signals along with the phase delay as the start of the crack has to be located exactly. After knowing the center of the crack (as discussed earlier), the magnitude of the longitudinal mode can be used to get the starting position of the crack. A better alternate method has to be devised for this purpose.

5.3   Characterization of Angular Crack

An attempt has been made to apply the present methodology to the cracks having different angular orientation than the circumferential nature.

36

Two cases have been tried for the cracks with orientation of 45° and 60° with respect to the axis of the tube. The geometry used for the angular cracks is shown in Figure 5.18 and 5.19. As mentioned earlier, the axial displacement variation on the circumference will not be symmetrical about any point for a crack with different orientation.

The axial displacements on the circumference for a crack of 45° is shown in Figure 5.20 while Figure 5.21 for a crack of 60°. Minimum displacement for 45° crack is at point 5 while for 60° crack, it is at point 3. Thus the point of minimum displacement goes on varying around the circumference depending upon the orientation of the crack. It is interesting to note here that the position of this point also has the effect of axial location. Therefore, it is difficult to exactly locate the angular location of the crack. Figure 5.22 and 5.23 show the displacement variation of these points respectively. The axial location of the crack is found to be at $65\mu s$ i. e., at $167mm$ from the front end.

The addition of the signals will not give the amplitude of the converted modes. Also because of angular nature of the crack, it may be possible that some other modes (similar to Rayleigh or surface waves) will be generated, as the pulse is not properly incident on the crack surface. A much detailed analysis using fine mesh has to be performed for these cases.
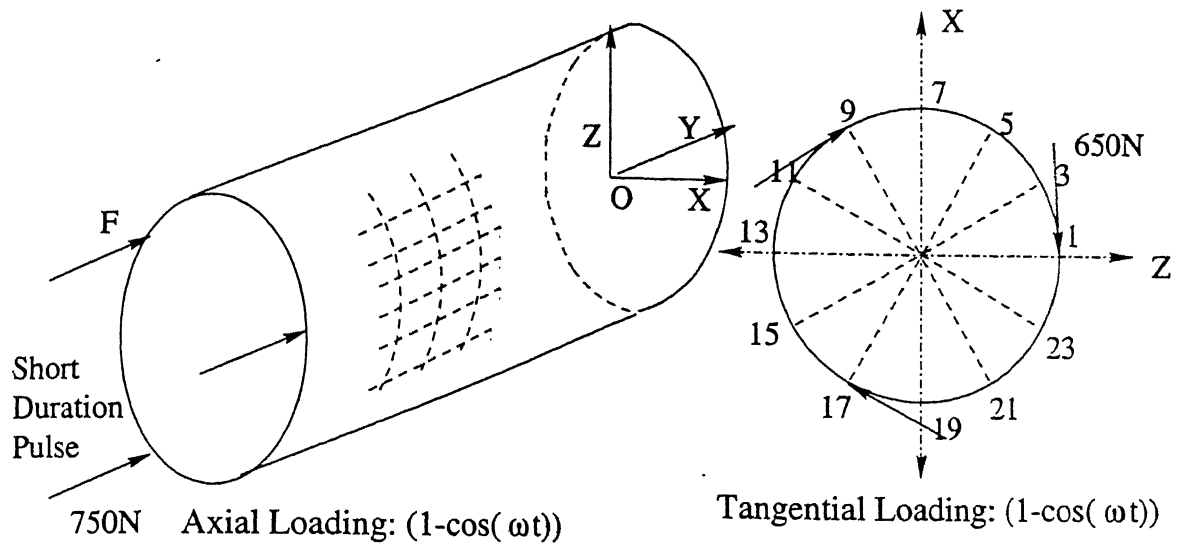
Figure 5.1: Loading used for Validation of the Code
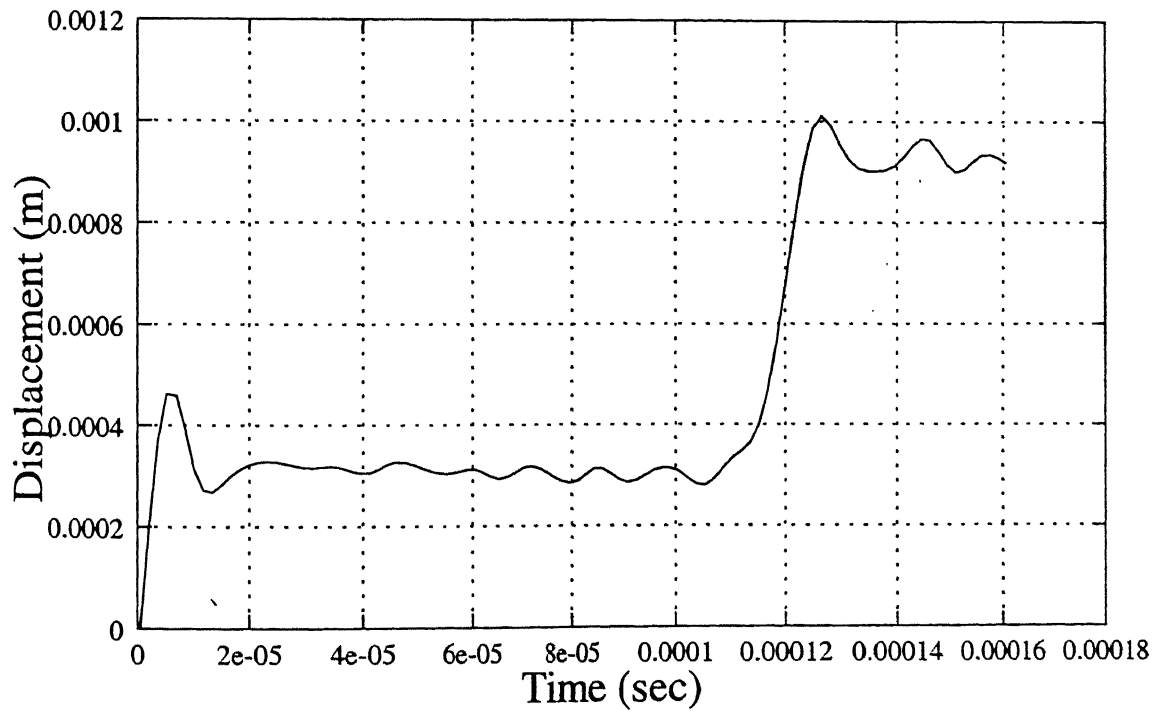
Figure 5.2: Axial displacement variation at one of the Loading point
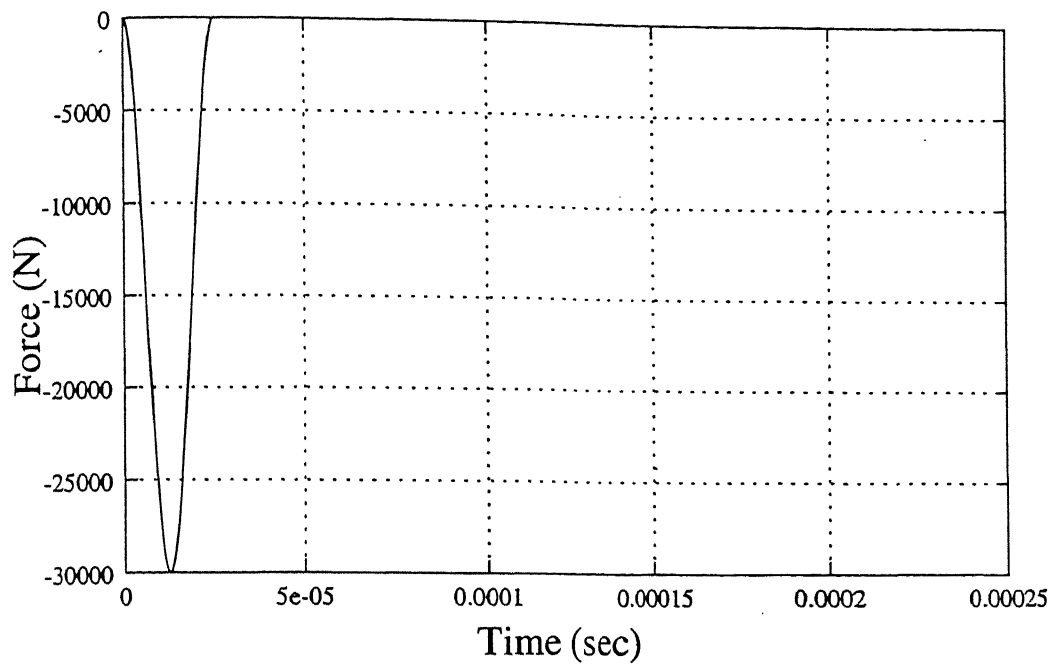
Figure 5.3: Input pulse at one of the loading point

24 Loading Points
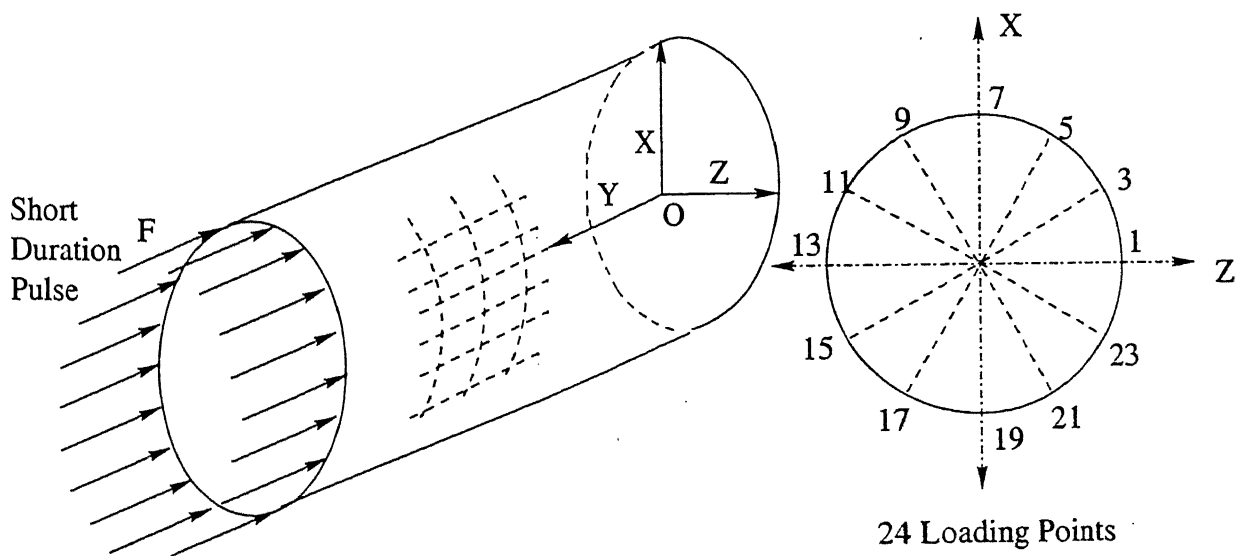
Figure 5.4: Crack free Specimen
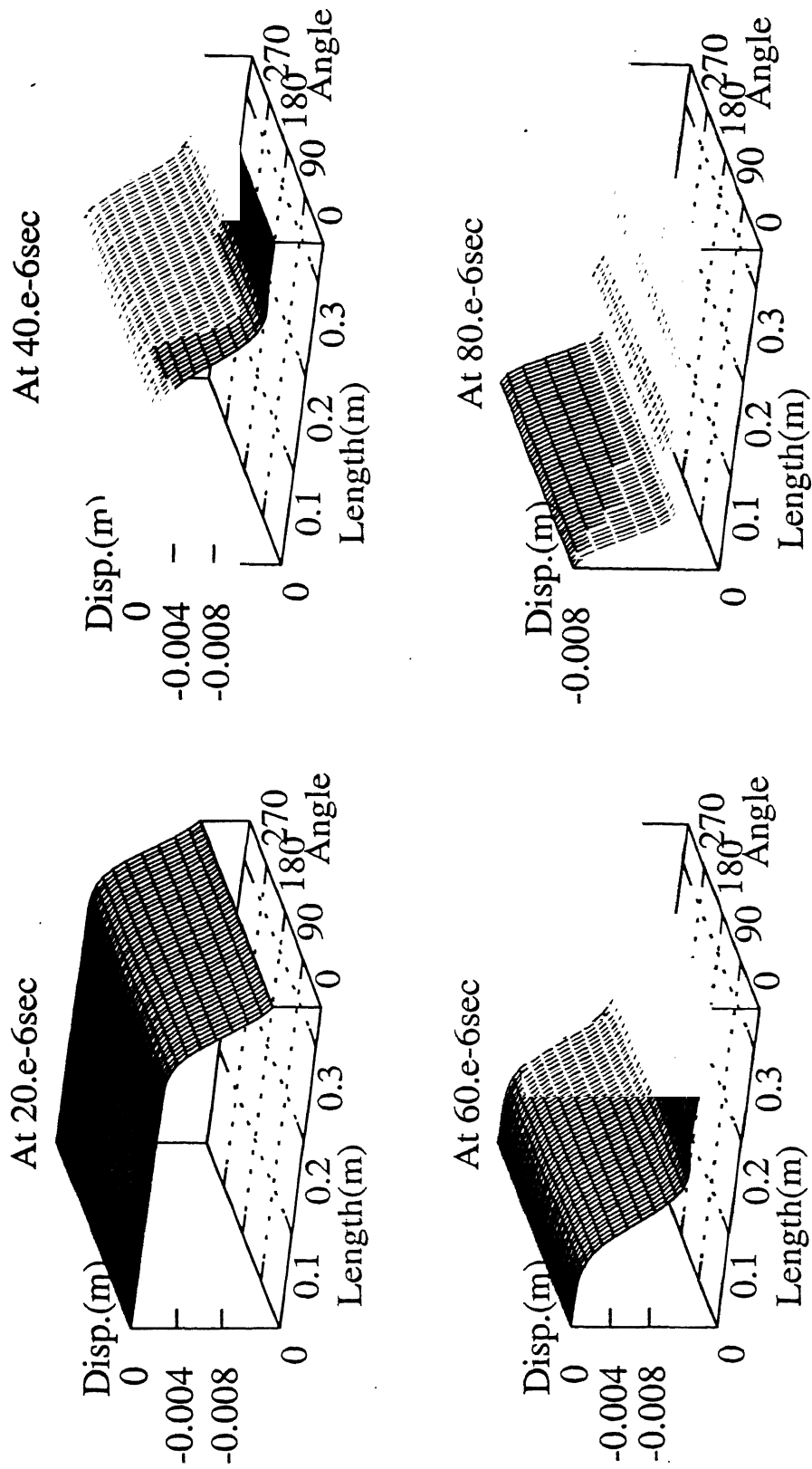
Figure 5.5: Snapshot of axial displacement on time domain (Crack free specimen)
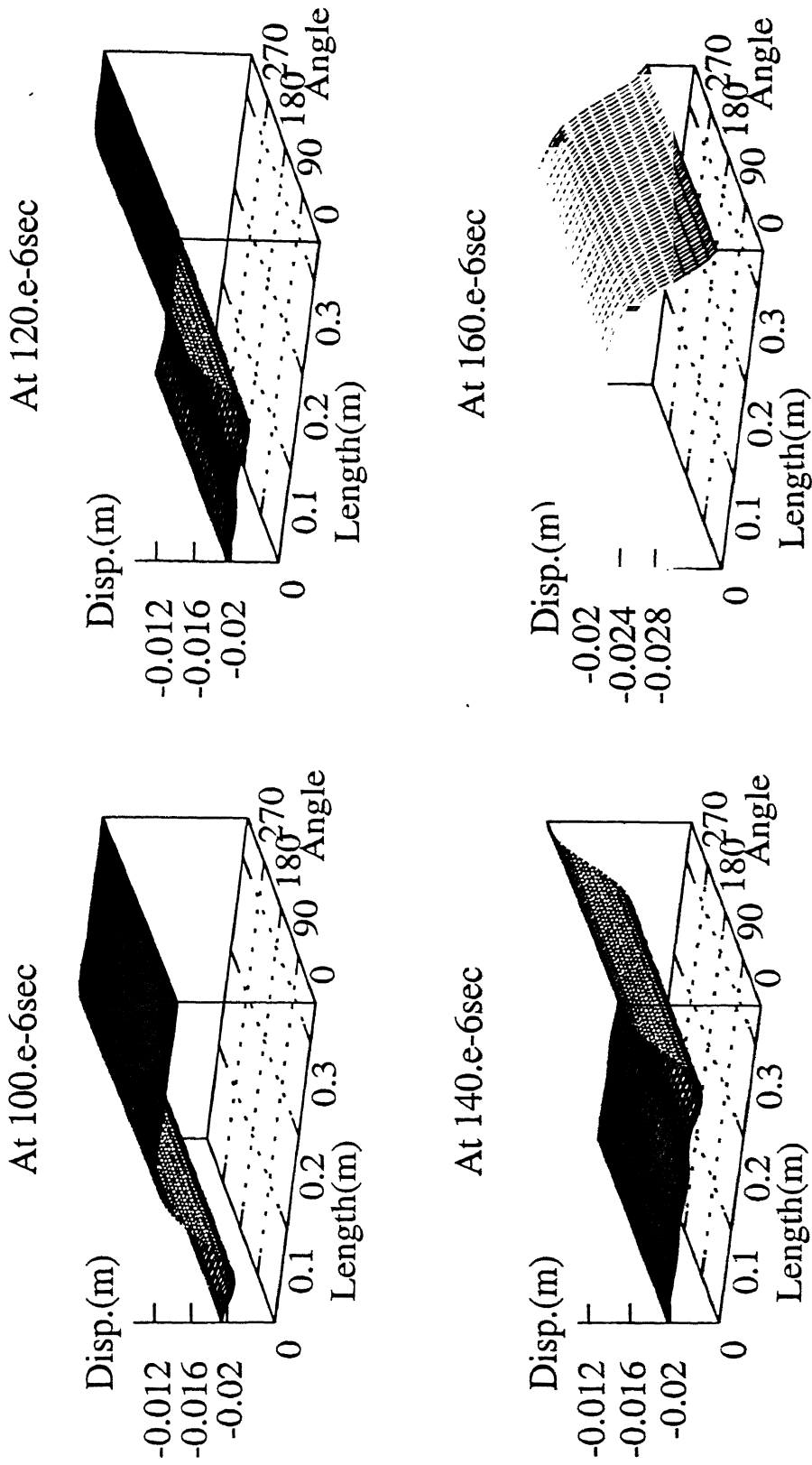
Figure 5.6: Snapshot of axial displacement on time domain (Crack free specimen)
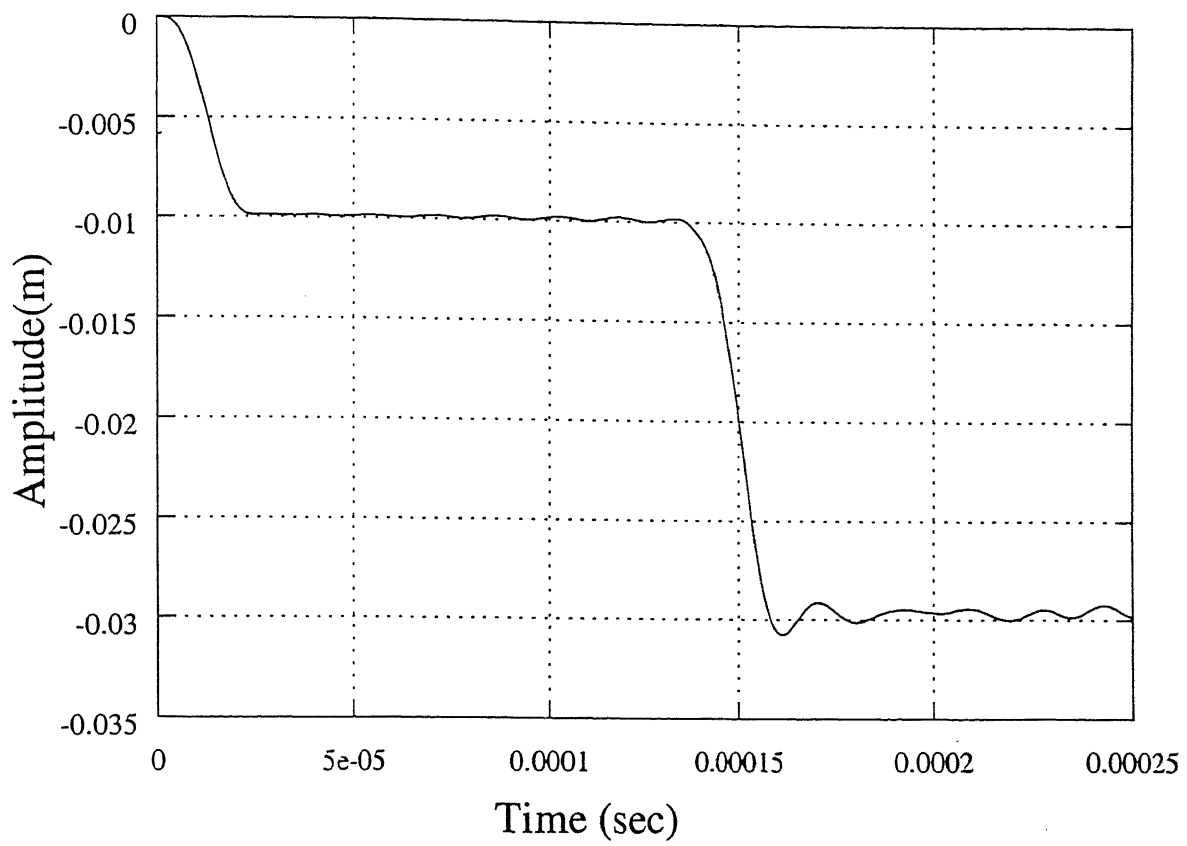
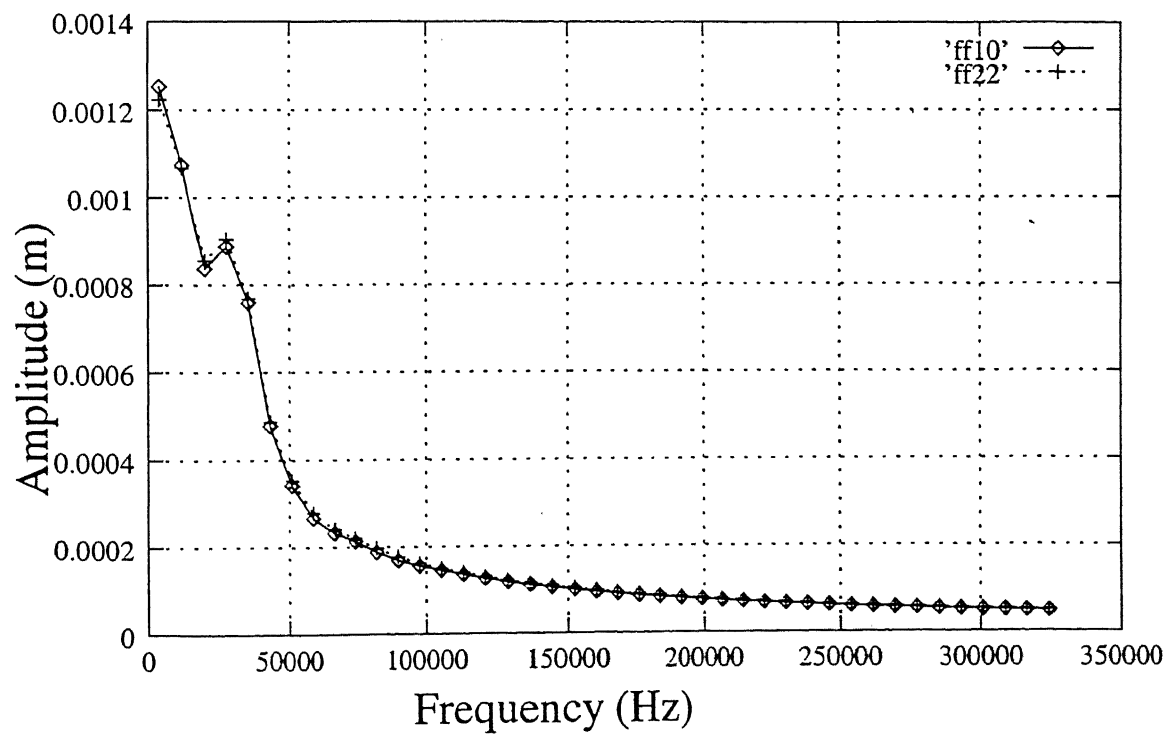Figure 5.7: Axial displacement variation at one of loading point (Crack free specimen)

Figure 5.8: Frequency domain amplitude for two points.
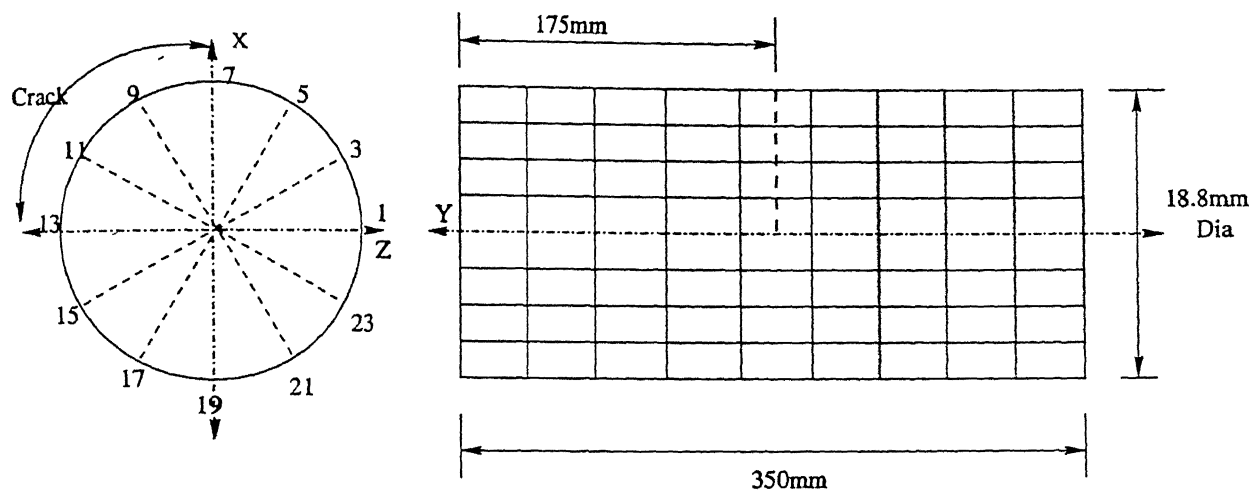
Figure 5.9: Geometry of circumferential crack at $175mm$ and 135°
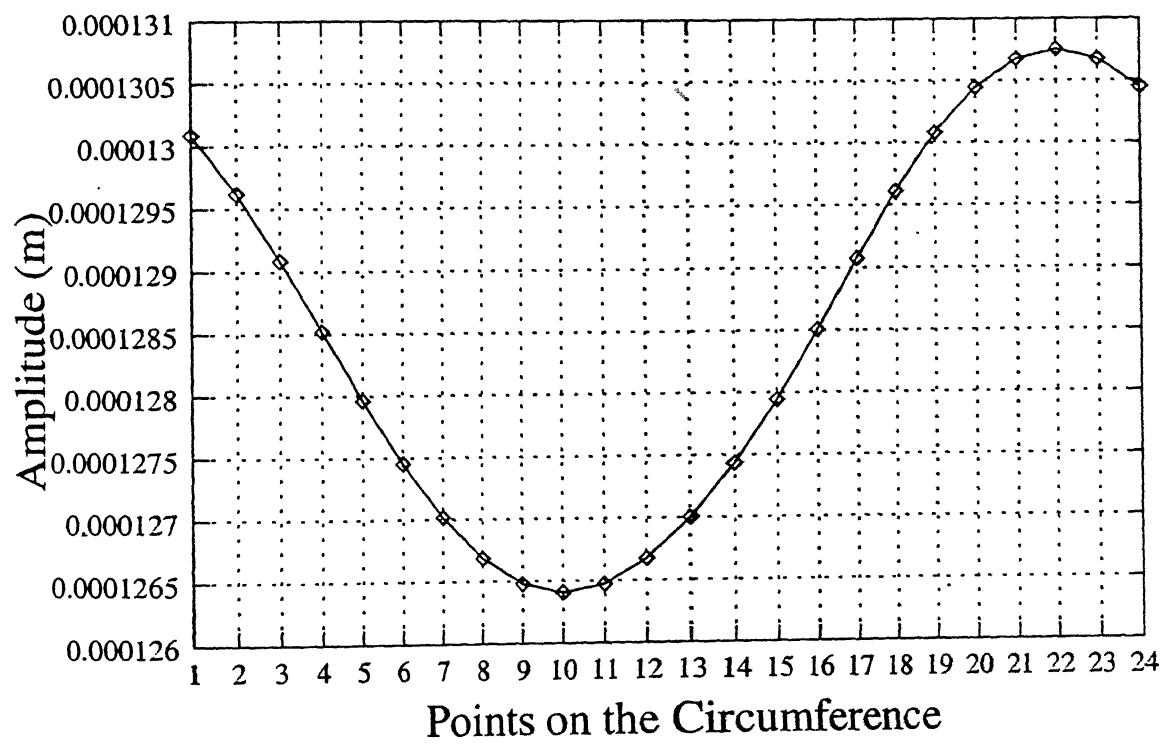
Figure 5.10: Axial displacement on the circumference (Circumferential crack $175mm$ and 135°)

43
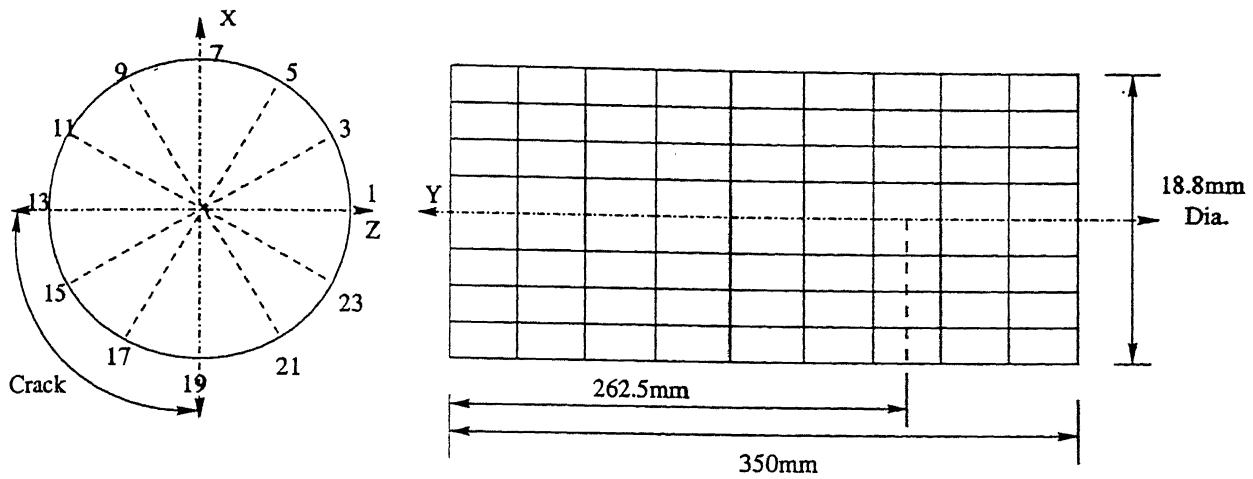
Figure 5.11: Geometry of circumferential crack at 262.5mm and 225°
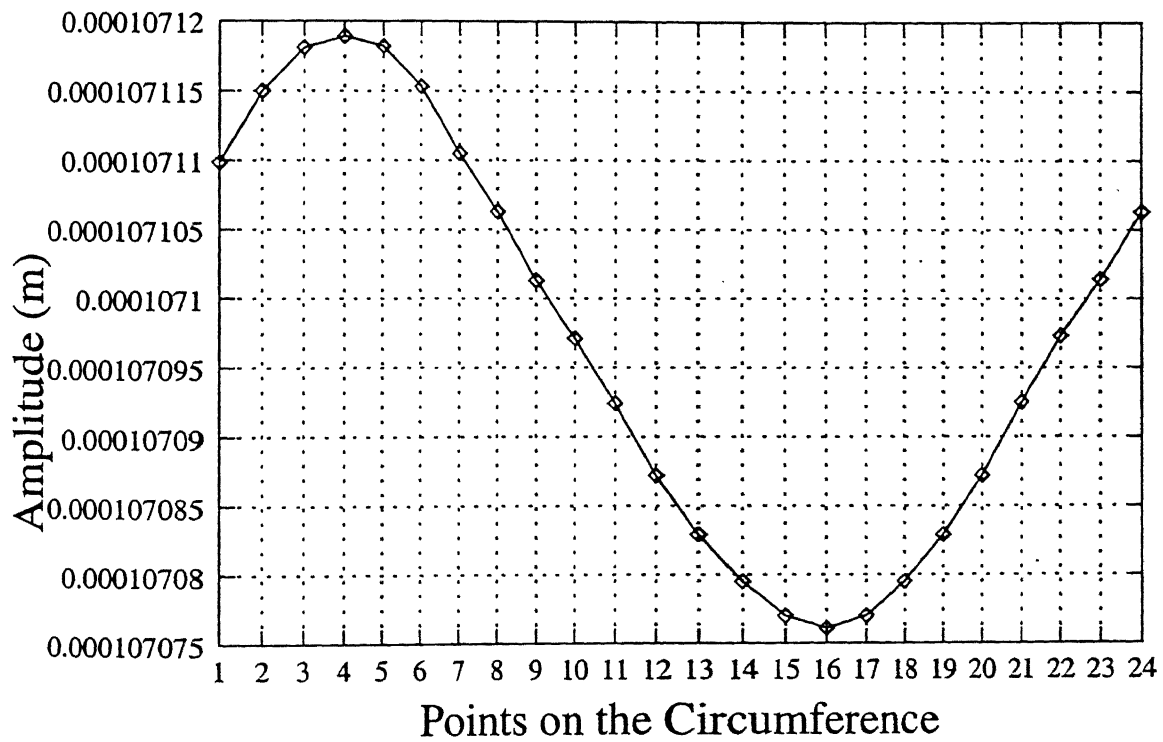
Figure 5.12: Axial displacement on the circumference (Circumferential crack 262.5mm and 225°)

44
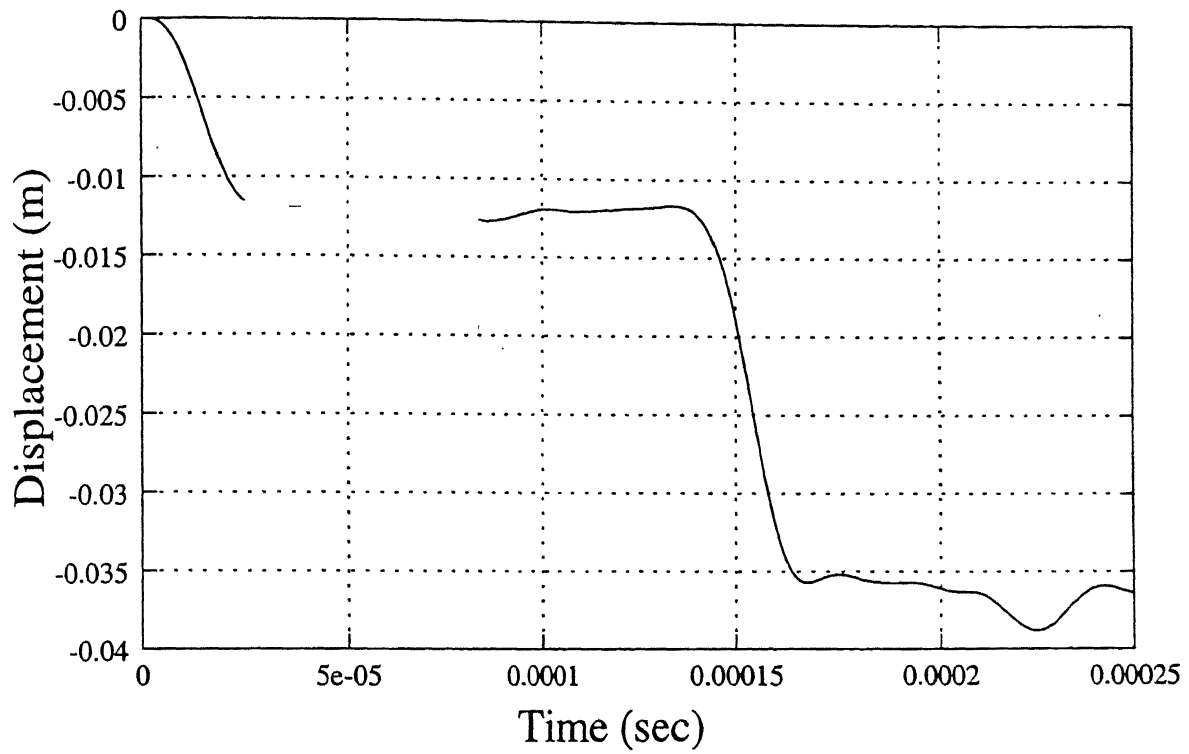
Figure 5.13: Axial displacement variation at point 10 (Circumferential crack at $175mm$ and $135°$)
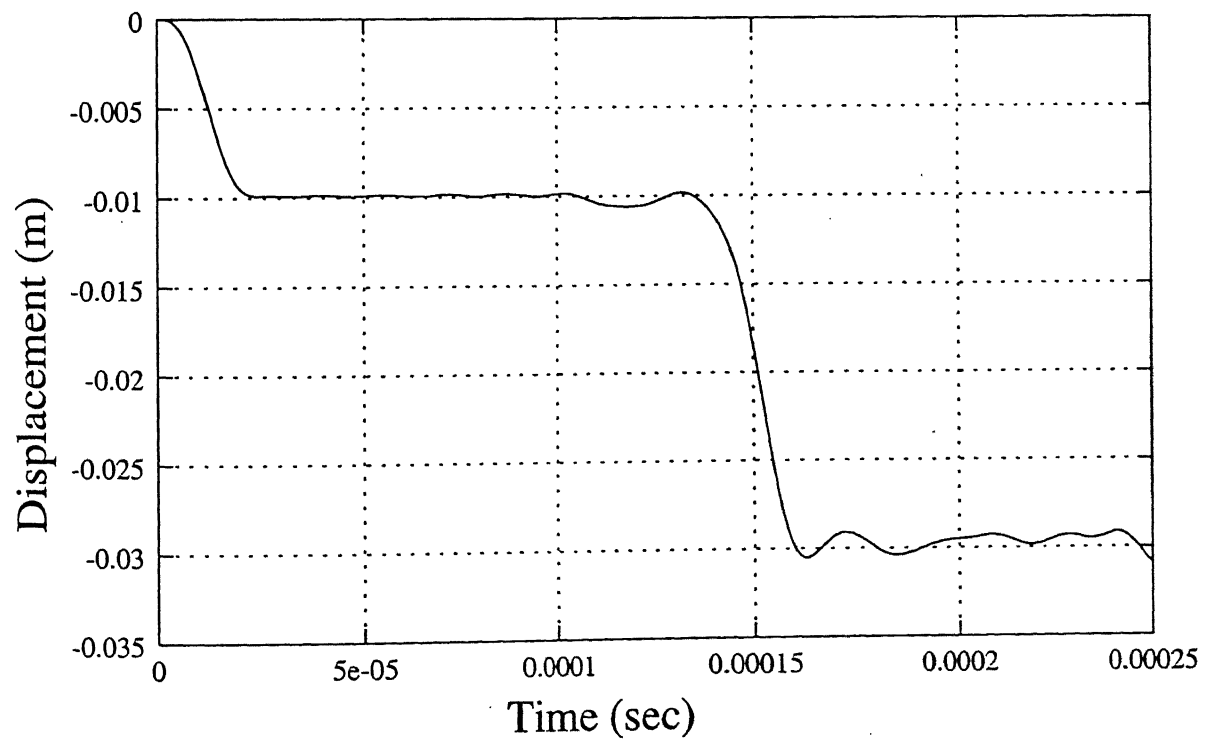
Figure 5.14: Axial displacement variation at point 16 (Circumferential crack at $262.5mm$ and $225°$)
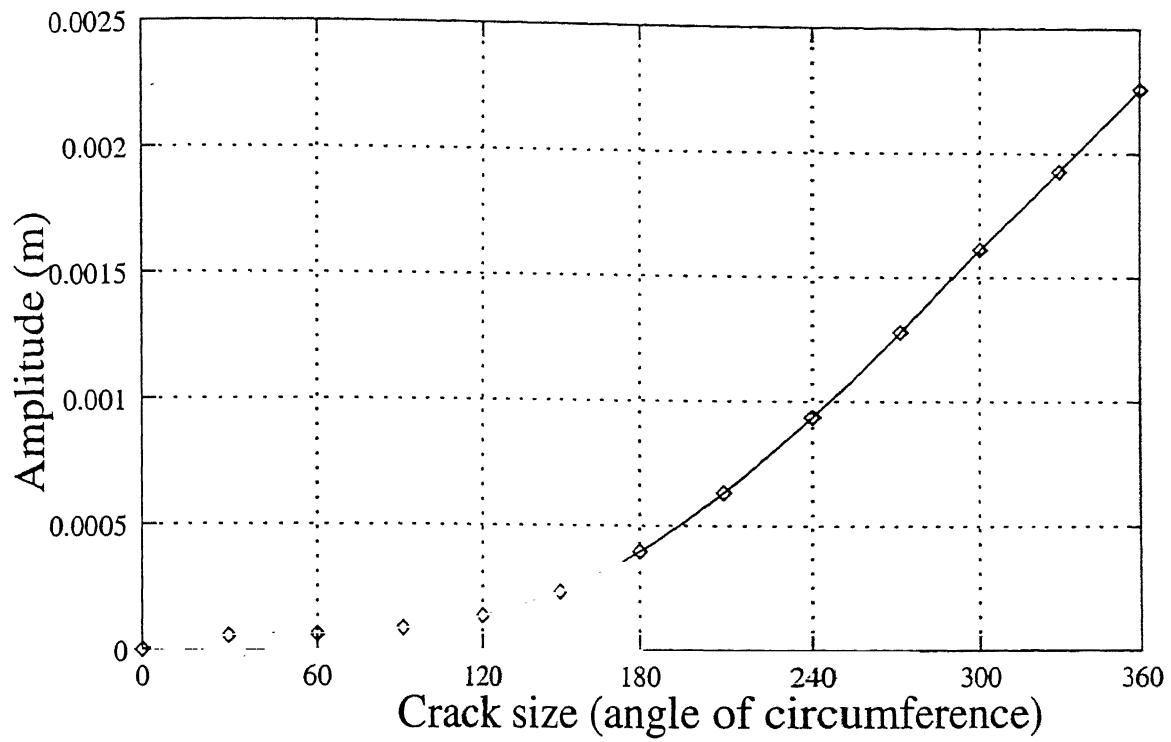
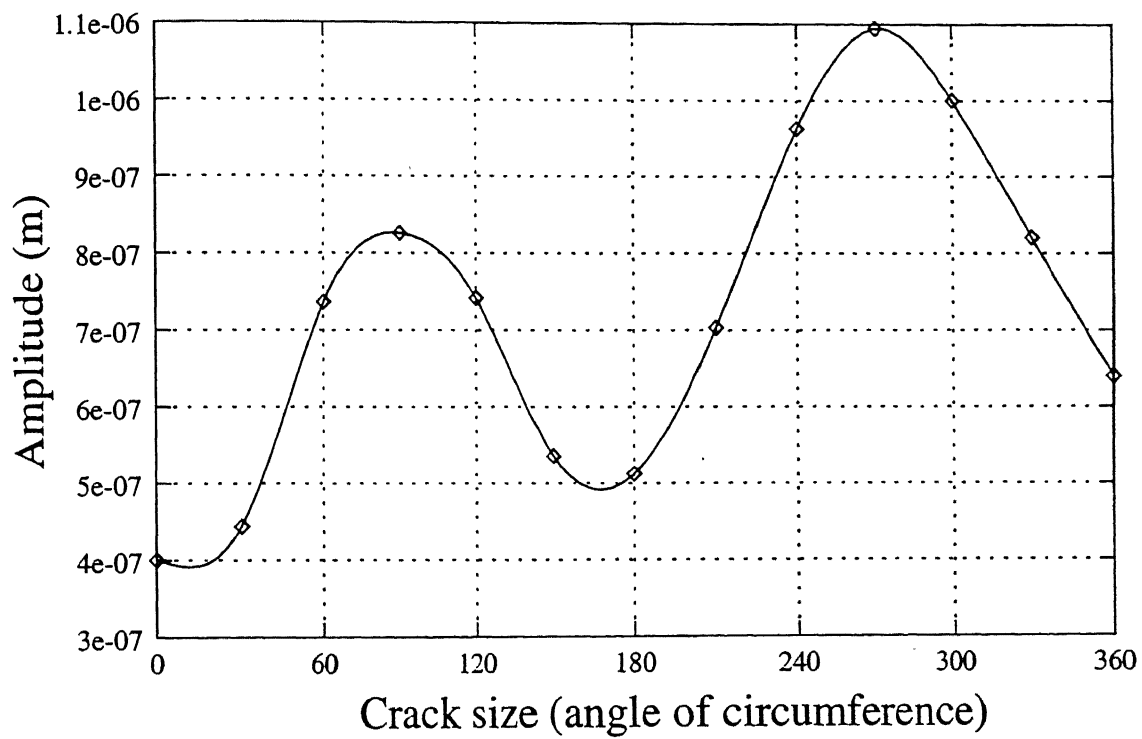Figure 5.15: L(0,2) Mode
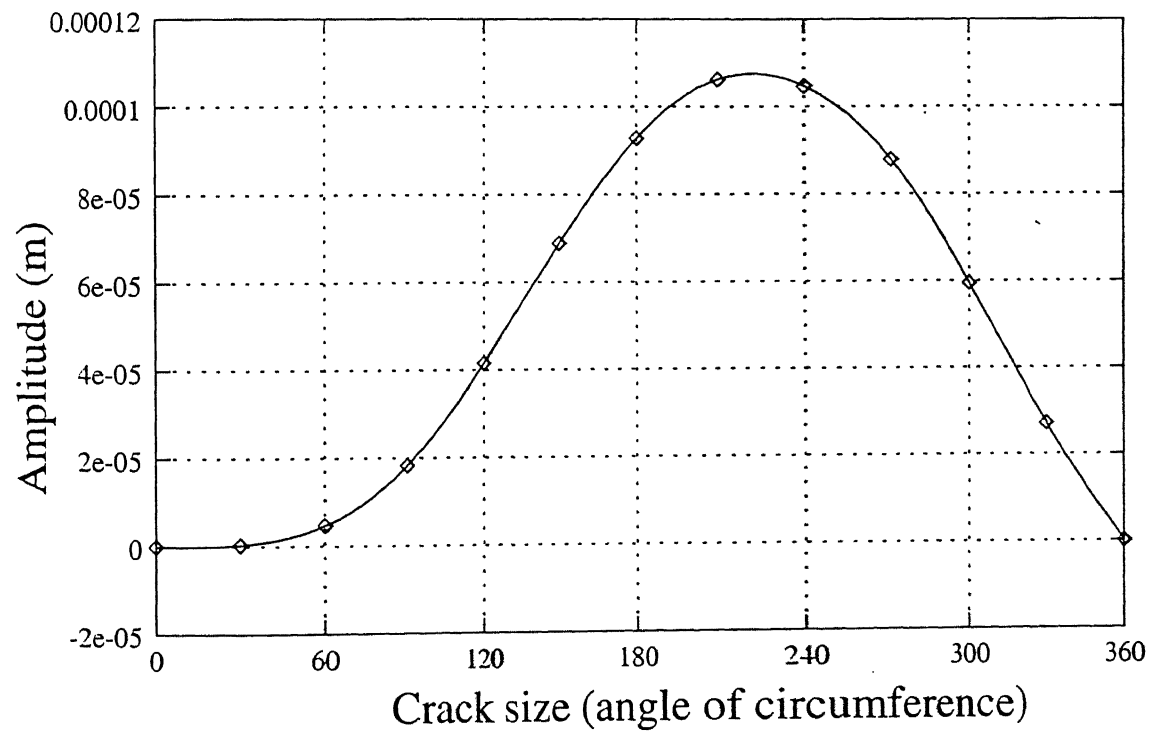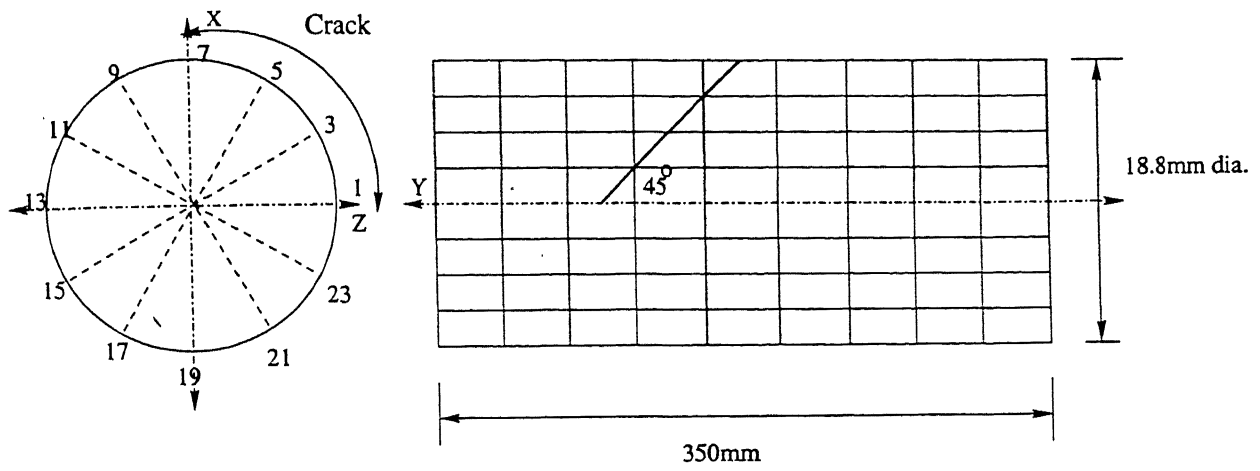

Figure 5.16: F(1,3) Mode

Figure 5.17: F(2,3) Mode

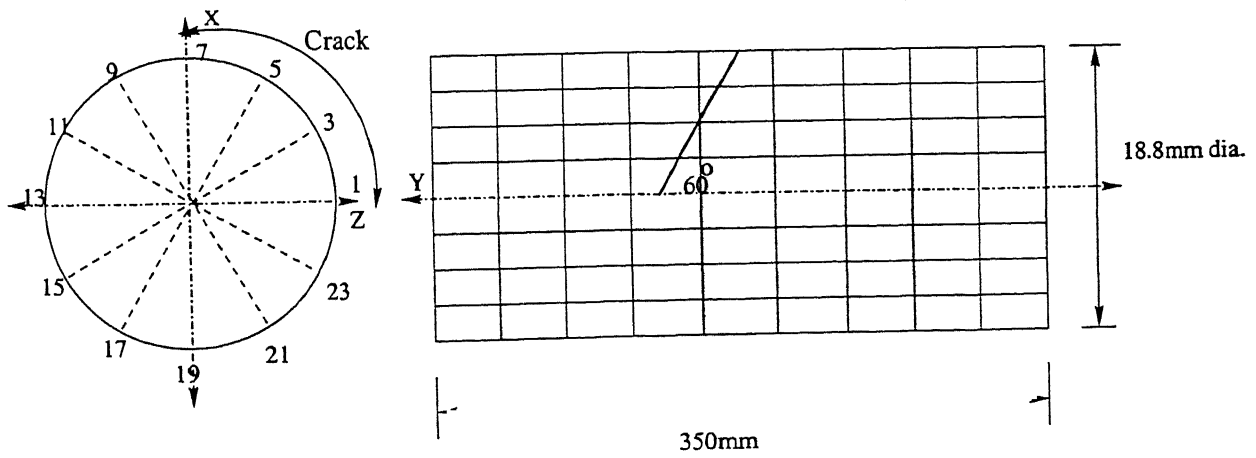Figure 5.18: Geometry of 45° Angular crack

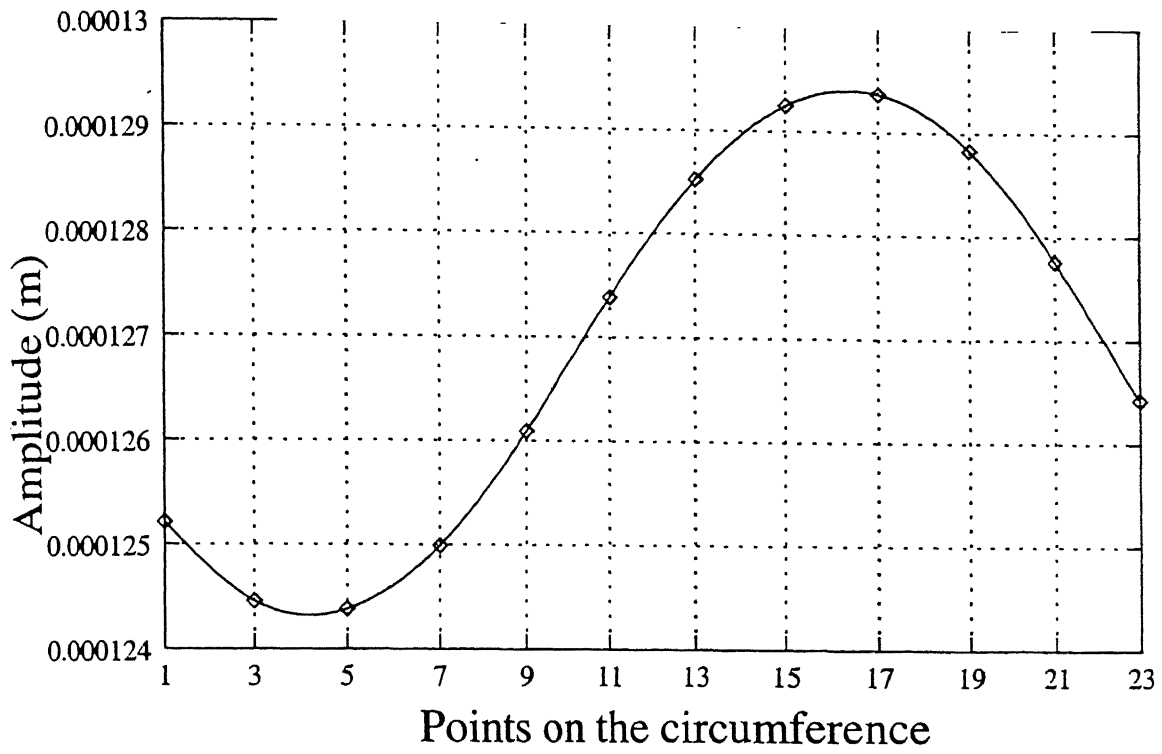Figure 5.19: Geometry of 60° Angular Crack

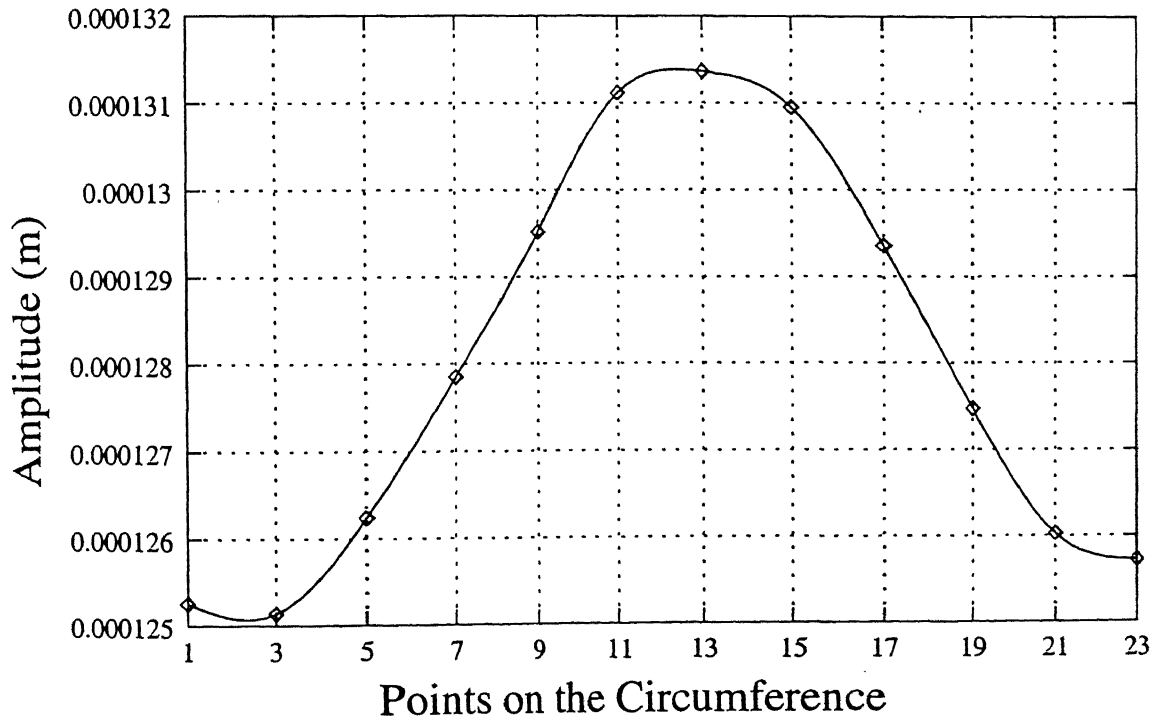Figure 5.20: Axial displacement on the circumference (45°Angular Crack)

Figure 5.21: Axial displacement on the circumference (60°Angular Crack)
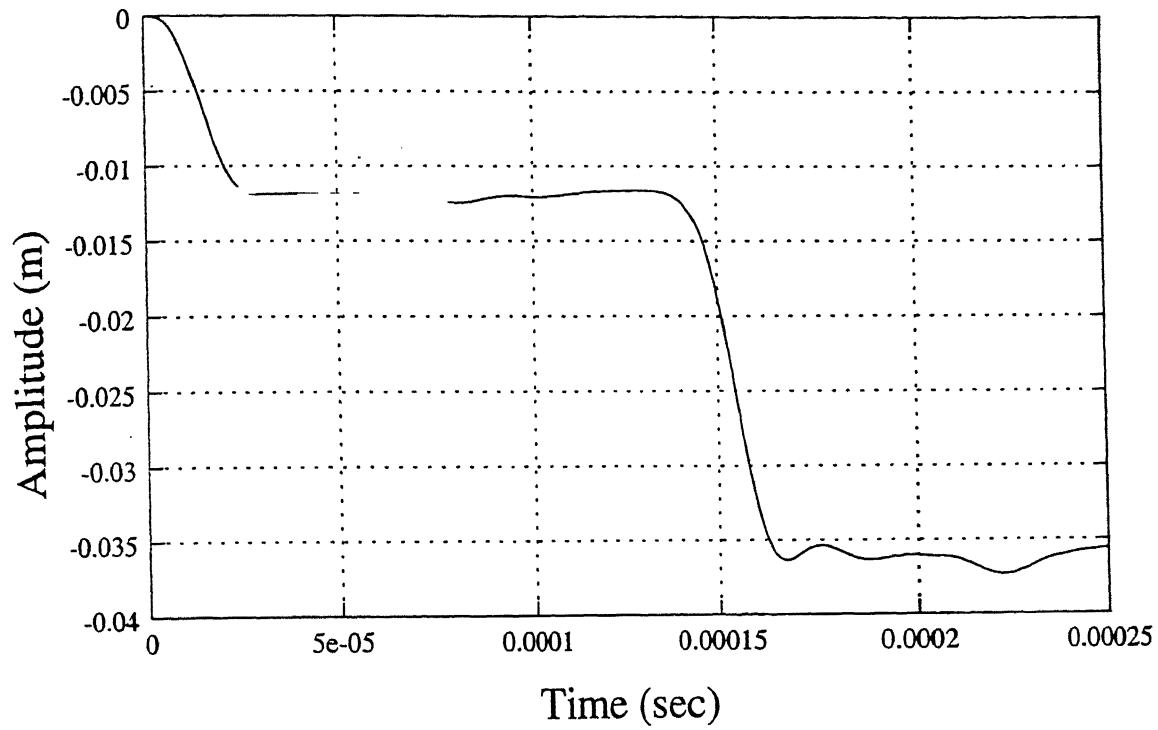
49

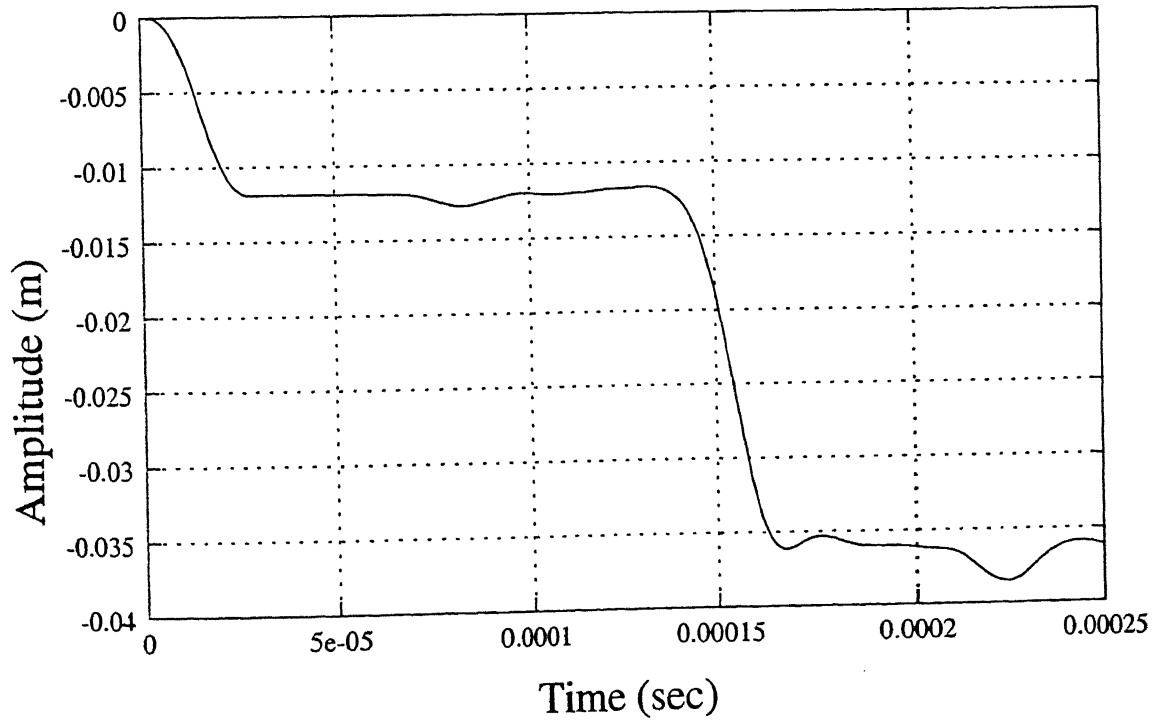Figure 5.22: Axial displacement variation of point 5 (45° Angular Crack)

Figure 5.23: Axial displacement variation of point 3 (60° Angular Crack)

Chapter 6

Conclusions

6.1 Conclusions

In the present work, an attempt has been made to use Finite element analysis and guided wave propagation phenomenon in tubes to characterize the cracks (through the thickness). Based on the results presented, in Chapter 5, the following conclusions can be drawn:

- The guided waves are found to be useful for the detection as well as characterization of defects.

- The methodology given in the present work is relatively simple than the earlier work [23] for the location of axial and the angular position of the cracks in the tubes. The presence of various modes of propagation can be used to know the size of the cracks.

- The longitudinal $L(0,2)$ mode is ideally suitable for the inspection of tubes because of the non-dispersive nature and highest phase velocity. The reflected $L(0,2)$ and the converted $F(1,3)$ and $F(2,3)$ modes contain good information about the defects.

- Linear variation of longitudinal mode to some extent reveals the size of the defect.

- Sinusoidal variation of flexural modes around the circumference reveals the suitability for non-axisymmetric crack. Flexural modes can be suitable than the longitudinal modes when the tube contain both axisymmetric and non-axisymmetric defects.

51

- For the inspection of very small cracks, the longitudinal modes can be replaced by flexural modes.

- It is difficult to study the mode conversion phenomenon for the cracks having angular orientation.

6.2   Scope for the future work

- For flexural modes, the addition of the amplitude requires exact start of the crack. Some effective method of addition has to developed to make it independent of starting position.

- For angular oriented cracks, a better mathematical model can be formulate to study the mode conversion phenomenon.

- The finite element model of the shell takes into account five degrees of freedom per node. This requires extensive computation in the numeric modeling. Some efforts can be tried to reduce some unwanted degrees of freedom for simpler computation.

References

1. D. C. Gazis. "Three Dimensional investigation of the Propagation of Waves in Hollow circular Cylinder," *J. Acoustic Soc. Am.*, Vol. 31, No. 5, pp. 568-578 (1959).

2. Fitch A. H. "Observation of Elastic Pulse Propagation in Axially Symmetric and Non-axially symmetric Longitudinal modes of Hollow Cylinders," *J. Acoustic Soc. Am.*, Vol. 35, pp. 706-708 (1979).

3. Peter Stepanishen and D. Ebenezer. "Transient vibratory response of fluid loaded shells with Axisymmetric Excitation," *J. Acoustic Soc. Am.* Vol. 82, No. 5, pp. 1811-1817 (1987).

4. Yves Brunetal, S. M. Candel. "Circumferential Propagation of SH waves in Hollow Cylinders," *J. Acoustic Soc. Am.*, Vol. 81, No. 4, pp. 840-843 (1987).

5. A.W.E. Neumann. "On the state of art of the Inspection of Acoustic welds with Ultrasound," *Int. J. of Pressure Vessels and Piping.* Vol. 39, No. 4, pp. 227-246 (1989).

6. D. Kalkhof, W. Görner, Ch. Schurig and Ch. Müller. " Detection of Defects in Acoustic pipings and welds of Nuclear Power Plant Components by Ultrasonics," *Int. J. of Pressure Vessels and Piping.* Vol. 39, No. 4, pp. 279-291 (1989).

7. Vikass Monebhurrun, Benard Duchene, D. Lesselier and Riadh Zorgati. "Eddy current Characterization of 3-D bounded Defects in Metal tubes using a Wavefield integral formulation modeling," *Nondestructive testing of Materials.* pp. 195-202 (1995).

8. K. Miya. "Progress of Tube Inspection Technology in Nuclear Power Plants of Japan," *Nondestructive testing of Materials*. pp. 341-347 (1995).

9. M. J. S. Lowe. "Matrix Technique for Modeling Ultrasound waves in Multilayered media". *IEEE Trans. Ultrasonics, Ferroelectric and Frequency Control*. Vol. 42, pp. 525-542 (1995).

10. M. G. Silk and K. F. Baiton "The propagation in metal tubing of ultrasound wave modes equivalent to Lamb waves," *Ultrasonic*, Vol. 17, pp. 11-19 (1979).

11. J. L. Rose, K. M. Rajana and F. T. Carr. "Ultrasonics guided wave inspection Concepts for Steam Generator Tubing," *Materials Evaluation*, Vol. 52, No. 2, pp. 307-310 (1994).

12. J. J. Ditri and J. L. Rose. "Excitation of guided wave modes in hollow cylinders by applied surface traction," *J. Acoustic Soc. Am.*, Vol. 72, pp. 2589-2597 (1992).

13. D. N. Alleyne and P. Cawley. "The excitation of Lamb waves in pipes using dry coupled piezoelectric transducers," *J. NDE.*, Vol. 15, pp.11-20 (1996).

14. D. N. Alleyne and P. Cawley. "The effect of discontinuities on long range on the long range propagation of Lamb waves in pipes," *J. Process Mechanical Engineering, Proc. I. Mech. E.*, Part E, Vol. 210, pp. 217-226 (1996).

15. D. N. Alleyne and P. Cawley. "The interaction of Lamb waves with defects," *IEEE Trans. Ultrasonics, Ferroelectric and Frequency Control*. Vol. 39, pp. 381-397 (1992).

16. R. C. Addison Jr., A. Safaeinili and A. D. W. Mckie. "Laser based Ultrasound for the Inspection of Gas Pipelines," *Review of Progress in Quantitative Nondestructive Evaluation*. Vol 16B. pp. 1277-1284 (1997).

17. J. L. Rose, J. J. Ditri, A. Pilarski. "Wave mechanics in Acousto-Ultrasonic Nondestructive Evaluation," *J. Acoustic Soc. Am.*, Vol. 12, No. 1, pp. 23-26 (1994).

18. D. N. Alleyne, M. J. S. Lowe, P. Cawley. "The Reflection of Guided Waves From Circumferential Notches in Pipes," *J. Appl. Mech. Vol. 65, pp. 635-641 (1998).*

19. J. L. Rose, J. N. Barshinger. "Development of Guided Waves For Adhesive Bond Inspection," *Quantitative Nondestructive Evaluation Conference, Bruswick, Maine.* (1996).

20. Hyeon Jae Shin, Michael J. Quarry, Josepf L. Rose. "Non-axisymmetric Guided Waves For Tubing Inspection," *Review of Progress in Quantitative Nondestructive Evaluation.* Vol 16B. pp. 1253-1260 (1997).

21. M. J. S. Lowe, D. N. Alleyne and P.Cawley. "The Mode Conversion of Guided Wave by a Part-Circumferential Notch in a Pipe," *J. App. Mech.* Vol. 65, pp. 649-656 (1998).

22. Joseph L. Rose, Dale Jiao and Jack Spanner, Jr. "Ultrasonic Guided Waves For Piping Inspection," *Review of Progress in Quantitative Nondestructive Evaluation.* Vol 16. pp. 1285-1289 (1998).

23. Ch. Ramakanth. "Finite Element Modeling of Guided Waves in Tubes For Inspection of Cracks," *(M.Tech. Thesis, Dept. of Mech. Engg. IIT Kanpur. 1998).*

24. J. D. Achenbach. "Wave Propagation in Elastic Solids." *(North Holland Publishing Company, Amsterdam. 1973).*

25. K. F. Graff. "Wave motion In Elastic Solids." *(Oxford University Press, U. K. 1975).*

26. Klaus Jürgan Bathe. "Finite element Procedures." *(Printice Hall of India. 1996).*

27. Robert J. Cook, David S. Malkus, Michael E. Plesha. "Concepts And Application of Finite Element Analysis." *(John Wiley & Sons. 1989).*

28. E. Hinton and D. R. J. Owen. "Finite Element Software for Plates and Shells." *(Pineridge Press, U. K. 1984).*